Electrostatic Confinement, Patterning and Manipulation of Charged Nanoparticles by Combining Nanostructured Surfaces and Ionic Charge Regulation

by

Ashwin Panday

A dissertation submitted in partial fulfillment
of the requirements for the degree of
Doctor of Philosophy
(Macromolecular Science and Engineering)
in The University of Michigan
2016

Doctoral Committee:

Professor L. Jay Guo, Chair
Research Scientist Pilar C. Herrera-Fierro
Professor Katsuo Kurabayashi
Professor Nils Walter

ACKNOWLEDGMENTS

As a graduate student, I always reminded myself that my primary goal was to make a unique contribution towards science. With great regard and respect, I thank all the people who have helped me with my research and have made sure that it was a pleasant and rewarding experience. I will take this opportunity to thank my advisor Dr. L. Jay Guo for his undying support, patience, and faith in me. In the past few years, I have known Professor Guo as a sympathetic, rational and principle centered person, not to forget his undying love for breakthrough research. His instructions, valuable ideas and continuous encouragement kept me motivated and will also do in the future. I would also like to thank my group members and Long Chen who not only complement my work with their ideas and analysis but also kept an eye on the progress of my work and introduced me to novel research methods. My research would not have been possible without their efforts and help. I would also like to thank the committee members for Professor Nils Walter, Professor Katsuo Kurabayashi, and Dr. Pilar HF for their guidance and serving on my committee. I am indeed grateful to my beloved parents, fiancé, family, friends and the Michigan community for their valuable suggestions, guidance and encouragement throughout these years.

PREFACE

Electrostatic forces are amongst the most versatile when applied to mediate the interactions between nanostructured interfaces. Depending on the experimental conditions, these forces can be either attractive or repulsive, and their directionality can be controlled dynamically. In this dissertation, we employ these forces to confine and manipulate charged nanoparticles using nanostructured interfaces. The various methodologies discussed herein inform and complement each other while opening pathways for diversified applications.

Electrostatic confinement of nanoscale species in solution has far-reaching effects in fields as diverse as biophysics, gene therapy, single-particle motion monitoring studies and bottom-up fabrication of nanostructures. We present a methodology to uniaxially confine charged nanoparticles on one-dimensional electrodes without the usage of geometrical barriers. An actively-tunable, engineered model system for electrostatic binding interactions is demonstrated and interaction characteristics are discussed in relation to mimicking the natural biological interaction between charged species. We further investigate the electrostatic interactions between nanoparticles and patterned sinusoidal-void structures. A size-selective nanoparticle confinement and patterning technique is demonstrated. In addition, ionic charge regulation in the electrical double layer, its ramifications and its applications are

discussed. In many particle-fractionation applications, complementary geometries are critical for understanding confinement characteristics and so a novel methodology is introduced to detect and visualize relative size variations in pre-characterized nanoparticle ensembles. This capped particle optical-sizing methodology is easily accessible, has high-throughput, and is relatively facile when compared to existing size-characterization techniques. Finally, a nanoparticle-manipulation-based transparent display concept is demonstrated that has been supplemented by our enhanced understanding of the above mentioned confinement methodologies of electrostatically confining charged nanoparticles in solution.

TABLE OF CONTENTS

LIST OF FIGURES

CHAPTER I

Introduction

1.1 Motivation and Objectives

Electric charge-field interactions at the nanoscale have been the corner stone of understanding many fundamental scientific phenomena and their applications encompass many interdisciplinary research areas like electrochemistry[1], solid-state electronics[2], semiconductor processing[3], macromolecular sciences and biophysics [4-7]etc. Electrostatic interactions between surfaces are prevalent in aqueous environments and their formation mechanisms and characteristics have been thoroughly studied and understood[8]. Based on various experimental conditions, these forces are extremely flexible and versatile and can be either attractive or repulsive, and their directionality can be controlled by tailoring the geometry of the interacting structures. In spite of these advances in research, there are many electrostatic interaction characteristics that need to be methodically demonstrated for applied research. This thesis presents experimental analyses and applications for confining and manipulating nanoparticles in solution using electrostatic fields.

Interactions between colloidal particles and structured surfaces have been exploited in various confinement and manipulation studies that rely primarily on fluid flow or geometric barriers[9,10]. Techniques that rely on the collective migration of species in response to external fields (electric or hydrodynamic, for example) are beset with difficulties including low precision, high electric fields, and dispersion limited resolution. Popular methods like dielectrophoresis and optical tweezing are hard to integrate and depend strongly on volumetric size, making them inadequate at the nanoscale[11]. Krishnan et. al demonstrated the geometry induced trapping of nanometric objects in fluidic slits but the system relies primarily on charged geometric barriers[10]. For biological systems, Minoura et al. experimentally demonstrated the one-dimensional diffusion and confinement of charged nanoparticles on biological microtubules based on charge regulation of the nanoparticles[12]. While many of these methods incorporate indirect methods of confining nanoparticles, actively controlled, direct charge-field interactions between charged entities are more versatile and can be tailored to specific applications.

One research area of interest is the interactions between charged nanoparticles (NPs) and biological macromolecules. For example, charged NPs interacting with a DNA backbone can change the electrostatic environment of the latter[13]. Another area

of interest is confinement and selective assembly of nanoparticles for bottom-up processing of materials.[14] In the research work presented here, we demonstrate how electrostatic interactions in artificially created systems can shed light on naturally occurring phenomena like the DNA-Protein interactions. We experimentally demonstrate the interaction characteristics and signify its versatility for applications in transparent fluidic displays. We also demonstrate how the electrostatic interaction can be tuned to selectively confine and assemble nanoparticles on a structured surface. As this research is influenced by the size of the nanoparticles involved, we have also developed a novel methodology for detecting relative size variations in nanoparticle ensembles.

1.2 Electrostatic interactions in an ionic solution

Most macromolecules as well as many oxide surfaces develop a net electric charge (by either the dissociation of chemical groups or the adsorption of ions from solution) when suspended in aqueous solutions[15]. Ionic charge separation in aqueous solutions is easily achieved with thermal energy (kT) surpassing the energetic barrier required for charge separation. Nanoparticles in solution also acquire a net electric surface charge by association or dissociation of charged species from solution. Similarly, an

electrode surface will acquire a net surface charge density when in contact with an aqueous solution due to the absorption or desorption of surface species. Electrolytes like ions and charged particles influence the distribution of ions near a surface. One set of ions that are opposite polarity to the charge on the surface screen the electrical charge forming an electrical double layer (EDL) as shown in the Figure 1.1 whose thickness is denoted by the Debye length (λ_D). Several models have been introduced to describe EDL in solutions. The Helmholtz model describes the EDL as two charged layer separated by a fixed distance. The Gouy-Chapman model illustrates the EDL as a surface charge and a charged layer in the fluid in which the shielding ions are diffused, named diffuse double layer. Another classical model is Gouy-Chapman-Stern model which combine the previous two models. Apart from the shielding ions in the fluid, an inner layer called Stern layer is added in the model. This inner part of the EDL is introduced to take into account the finite size of ions which limits the thickness of the inner boundary of the diffuse part of the EDL as the center of an ion can only approach the surface to within its hydrated radius. As indicated in Figure 1.1, the potential at the Stern plane defined as the center plane of the Stern layer is close to the electrokinetic potential or the zeta potential (ζ) at solid-liquid interface.

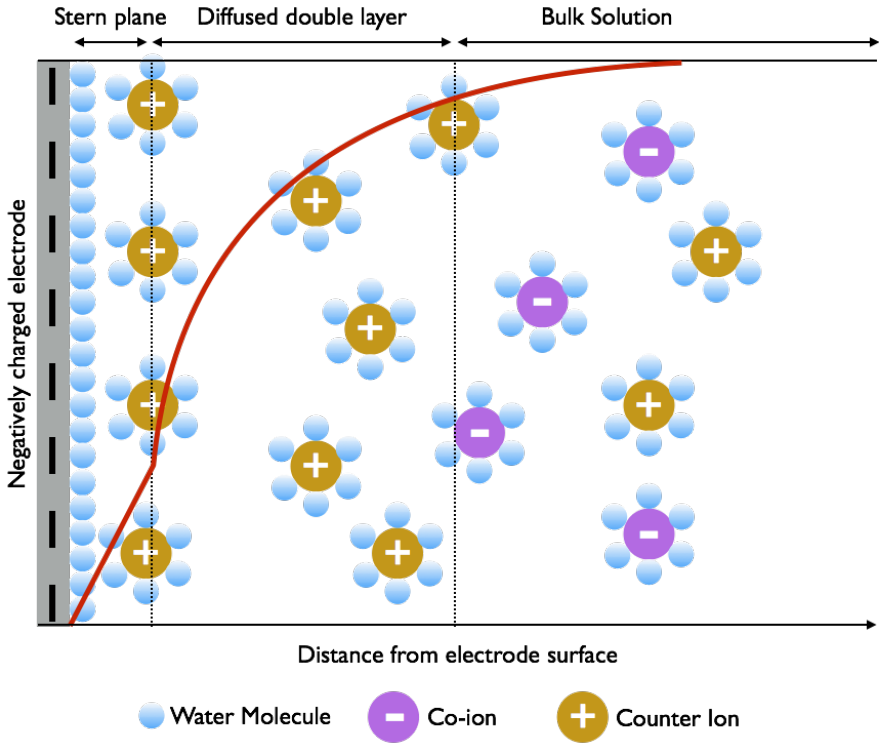

Figure 1.1: Structure of the electrical double layer at a negatively charged surface with co-ions and counter-ions hydrated with water molecules. Red curve shows the potential decay from the interface into the bulk of solution.

Under experimental conditions, because of the thermal motion of ions and molecules at room temperature, these ions have enough energy to overcome the electrostatic potential energy and escape from the EDL[16]. This creates a diffused layer of ions near a surface whose edge leads to a characteristic distance known as the screening Debye length, λ_D, which is expressed as, for a 1:1 electrolyte,

$$\lambda_D = \sqrt{\frac{\epsilon_0 \epsilon_r kT}{2z^2 qF c_b}}$$

where ε_0 is permittivity in vacuum, ε_r is the dielectric constant of the liquid, kT is thermal energy, c_b is the bulk molar concentration of the ionic solution, z is its valency, and F is Faraday's constant (9.648 70 x 10^4 C mol^{-1}). The Debye length depends solely on the properties of the liquid and not on any property of the surface such as its charge or potential (ψ). This ionic concentration gradient extends several nanometers into the bulk of solution and depends on the ionic strength of the solution. Because most of the interfacial charge is screened within the EDL, the thickness of the EDL is also the length scale of interaction between charged species in ionic solutions. The EDL depends solely on the properties of the liquid and not on any property of the surface such as its charge or potential.

1.3 Mimicking biological interactions in an artificial system

The living cell symbolizes the pinnacle of natural design and, its evolution over billions of years has made sure that fundamental processes like sensing and actuation are carried out at the nanoscale with great efficiency and precision, far beyond the capabilities of man-made, artificial systems. One of the most powerful of such processes is the transcription of DNA into RNA. In 1965 Sir F.C. Crick proposed that the central dogma of biology was to completely understand how the DNA-protein

interactions lead to the process of transcription[17]. In this system, the string of instructions encoded in a DNA sequence is "sensed" by a specific protein, and the actuation consists of the utilization of energy stored in pyrophosphate (and phosphodiester) bonds to transcribe a new string of RNA molecules with high speed and specificity[18]. Moreover, this astonishingly powerful system uses benign conditions and mundane physical forces: "simple" electrostatic interactions, Van Der Waals interactions, hydrophobic, and hydrogen bonding. In its simplest form, RNA transcription follows these steps[19] :

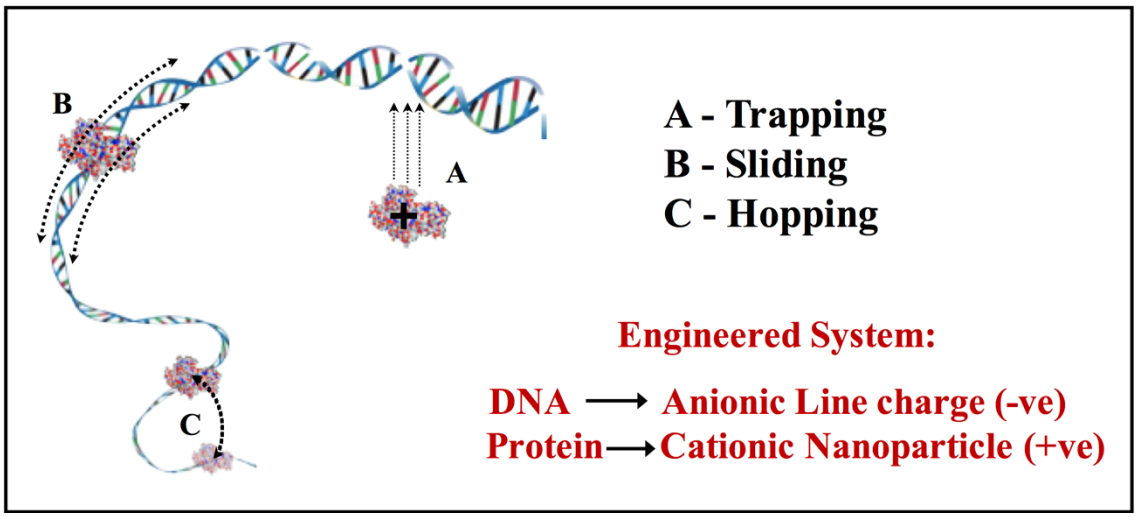

Figure 1.2: Modes of cationic protein transport while searching for target sites on a DNA backbone. Representation of this interaction in an artificial system.

(1) RNA polymerase (RNAP), a protein molecule, binds to the DNA at a nonspecific

location and searches for the promoter DNA sequence via a one-dimensional diffusion process known as "facilitated diffusion"[20].

(2) RNAP binds to the promoter with a specific DNA sequence and initiates RNA synthesis[21].

Although, this behavior has been visualized in-vitro by Larson et al.[22], fundamental principles, parameters and synchronous biological activity that govern this complex interaction remain mysterious. Over the past few decades, research groups have proposed [23] and theorized [24]that non-specific electrostatic attraction between the cationic residues on the proteins and the negatively charged phosphate groups on the DNA backbone play an important role in this targeting process. If this picture is correct, then a positively charged macromolecule should also be attracted to a synthetic mimic of the DNA, non-specifically, and in principle might also undergo one-dimensional diffusion. Surprisingly, even a "simple" system like this is yet to be replicated synthetically. An equally interesting question is whether there are any predictable scaling properties that can be deduced by comparing two systems that have different sizes and charge densities. We intended on creating an artificial system that mimics the above-mentioned aspects of a DNA-Protein (DP) interaction using non-biological nanostructures. Utilizing the principles of active, electrostatic particle

confinement, we visually recreate this interaction in our experiments and the results provide strong evidence that fundamental Coulombic interactions are capable of playing a primary role in this process. We envisage that our analysis will shed some light on the charge related nuances of this complex interaction. The methodology presented herein may find applications in nanoparticle confinement, assembly, manipulation, genomic analyses and single molecule DP interaction studies at low ionic strengths.

Since the original observation that the lac repressor protein is able to locate its DNA target site faster than the Smoluchowski diffusion limit [25], research groups have proposed that DP interactions are interplay between long-range electrostatic, and short-range forces. Minoura et al. experimentally demonstrated the 1-D diffusion of charged nanoparticles on biological microtubules and it was shown that non-specific electrostatic interactions were sufficient to cause this behavior. Charge on the DNA, charge on the protein, relative size, conformation, and physiological ionic strength of the interacting medium play a key role and the interaction is favorable only when these parameters strike a balance. To replicate the electrostatic aspect of this interaction, we model the DNA as one dimensional line charge (1-D) and the protein as a charged nanoparticle dispersed in an ionic solution. Hopping and sliding motion

during the DP interaction, in a natural system, translates to trapping/de-trapping and 1-D diffusion of nanometric objects, in a synthetic system. Usage of line charges is of paramount significance as they replicate the natural system both geometrically (relative sizes of DNA and interacting protein enzyme) as well as electrostatically. In our synthetic system, these structures help with reducing non-specific binding events and creating a 1-D electrostatic potential well to confine charged particles in the direction transverse to the 1-D line charge. This concept of dimensionality is relevant in a natural system as the DNA backbone is highly negatively charged (2e-/3.4A°) [26]

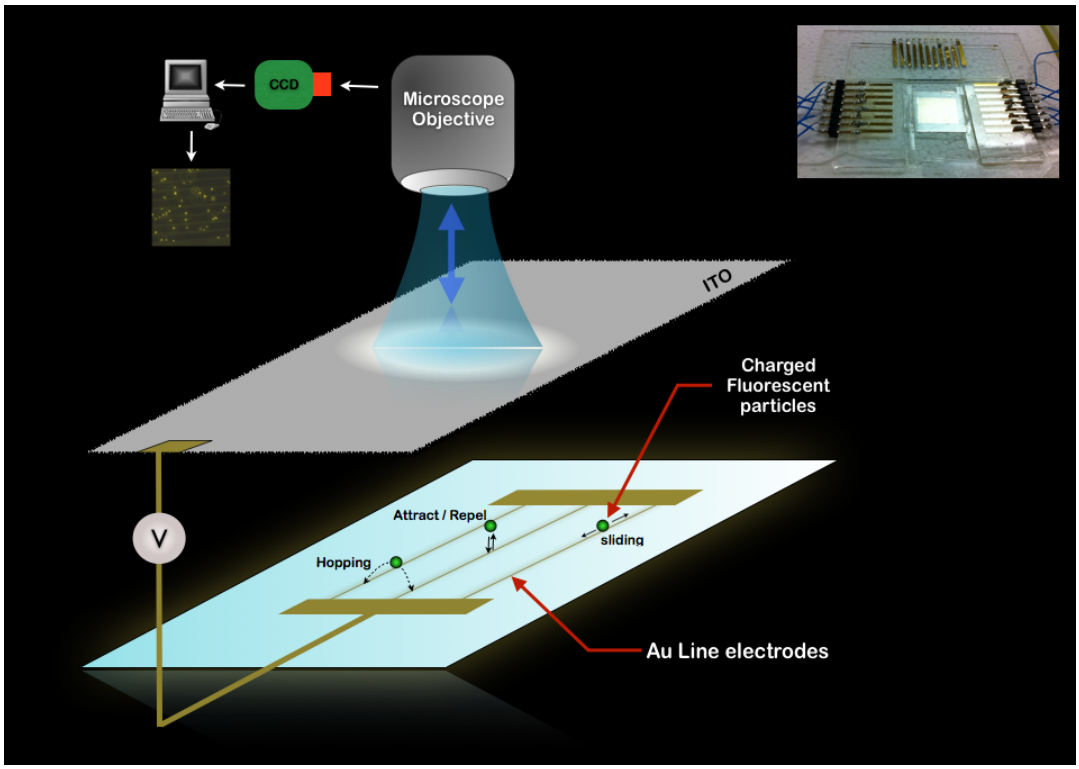

Figure 1.3: Schematic design for replicating the characteristics of a DP biological interaction in an engineered system

and has a diameter of ~2nm whereas the protein (LacI repressor) has a hydrodynamic radius of 5nm and +18e^- charges14. The surface potential on the DNA was reported to be periodic 13and so in essence the DNA behaves like a cylindrical line charge to the binding protein enzyme. In our synthetic system, the 1-D line charge is realized by fabricating a metallic nanowire, whose surface charge density as well as polarity can be dynamically controlled at will by an applied voltage. This idealized system helps to pronounce the electrostatic aspect of a DP interaction, while muting other potential secondary interactions as represented our schematic in Figure 1.3. While our system portrays the intricate DP interaction as a simple and idealized electrostatic interaction, if proven to be accurate, it could have a large and long lasting impact on our understanding of these interactions that have been mulled over for the past four decades.

1.4 Thesis Organization

There are four major chapters that discuss the confinement, assembly and manipulation of charged nanoparticles in solution and their applications, prefaced by an introduction to concepts and a final conclusion and future outlook. Chapter II introduces the uniaxial confinement of charged nanoparticles in solution and its

relevance to mimicking biological interactions in an artificial system. Chapter III details how the electrostatic interaction can be tuned to confine and assemble nanoparticles on geometrically charged and nanostructured surfaces. Chapter IV follows the issues faced in chapter III and introduces a new methodology for detecting relative size distribution in a nanoparticle ensemble and finally Chapter V discusses and demonstrates electrostatic confinement and manipulation for applications in transparent displays. These chapters shed light on some key insights that accentuate our understanding and applicability of electrostatic interactions. Some parts of this thesis have been reproduced from our publications in research journals and have been appropriately referenced.

1.5 References

1. Ammam, M. Electrophoretic deposition under modulated electric fields: a review. RSC Adv. 2, 7633–14 (2012).
2. Cheng, L.-J. & Guo, L. J. Rectified ion transport through concentration gradient in homogeneous silica nanochannels. Nano Lett. 7, 3165–3171 (2007).
3. Ruzyllo, J. Semiconductor Cleaning Technology: Forty Years in the Making. (The Electrochemical Society interface, 2010).
4. Green, N. G., Morgan, H. & Milner, J. J. Manipulation and trapping of sub-micron bioparticles using dielectrophoresis. Journal of Biochemical and Biophysical Methods 35, 89–102 (1997).
5. Rahman, K. M. A., Durning, C. J., Turro, N. J. & Tomalia, D. A. Adsorption of Poly(amidoamine) Dendrimers on Gold. Langmuir 16, 10154–10160 (2000).
6. GUERON, M. & DEMARET, J. P. A Simple Explanation of the Electrostatics of the B-to-Z Transition of DNA. Proc. Natl. Acad. Sci. U.S.A. 89, 5740–5743 (1992).
7. Buzea, C., Pacheco, I. I. & Robbie, K. Nanomaterials and nanoparticles: Sources and toxicity. ArXiv.org physics.med-ph, (2008).
8. Walker, D. A., Kowalczyk, B., la Cruz, de, M. O. & Grzybowski, B. A. Electrostatics at the nanoscale. Nanoscale 3, 1316–29 (2011).
9. Cohen, A. E. & Moerner, W. E. Suppressing Brownian motion of individual biomolecules in solution. Proc. Natl. Acad. Sci. U.S.A. 103, 4362–4365 (2006).
10. Krishnan, M., Mojarad, N., Kukura, P. & Sandoghdar, V. Geometry-induced electrostatic trapping of nanometric objects in a fluid. Nature 467, 692–695
11. Single-molecule force spectroscopy: optical tweezers, magnetic tweezers and atomic force microscopy. 5, 491 (2008).
12. Minoura, I., Katayama, E., Sekimoto, K. & Muto, E. One-Dimensional Brownian Motion of Charged Nanoparticles along Microtubules: A Model

System for Weak Binding Interactions. Biophysj 98, 1589–1597 (2010).
13. Halford, S. E. How do site-specific DNA-binding proteins find their targets? Nucleic Acids Research 32, 3040–3052 (2004).
14. Li, F., Josephson, D. P. & Stein, A. Colloidal Assembly: The Road from Particles to Colloidal Molecules and Crystals. Angew. Chem. Int. Ed. 50, 360–388 (2010).
15. Bockris, J. O. & Reddy, A. K. N. Modern Electrochemistry. (Springer Science & Business Media, 2012). Doi: 10.1007/978-1-4613-4560-2
16. Cheng, L.-J.Larry.Ion and Molecule transport in nanochannels. 1–173 (2008).
17. CRICK, F. Central Dogma of Molecular Biology. Nature 227, 561–563 (1970).
18. Facilitated target location in biological systems. 264, 675–678 (1989).
19. Mahmutovic, A., Berg, O. G. & Elf, J. What matters for lac repressor search in vivo—sliding, hopping, intersegment transfer, crowding on DNA or recognition? Nucleic Acids Research 43, 3454–3464 (2015).
20. Berg, O. G., Winter, R. B. & Hippel, Von, P. H. Diffusion-driven mechanisms of protein translocation on nucleic acids. 1. Models and theory. Biochemistry 20, 6929–6948 (1981).
21. Vinson, V. Real-Life Transcription Factor Dynamics. Science's STKE 2007, tw190–tw190 (2007).
22. Kim, J. H. & Larson, R. G. Single-molecule analysis of 1D diffusion and transcription elongation of T7 RNA polymerase along individual stretched DNA molecules. Nucleic Acids Research 35, 3848–3858 (2007).
23. Cherstvy, A. G., Kolomeisky, A. B. & Kornyshev, A. A. Protein−DNA Interactions: Reaching and Recognizing the Targets. J. Phys. Chem. B 112, 4741–4750 (2008).
24. Florescu, A.-M. & Joyeux, M. Description of nonspecific DNA-protein interaction and facilitated diffusion with a dynamical model. J. Chem. Phys. 130, 015103 (2009).
25. Riggs, A. D., Lin, S. & Wells, R. D. Lac Repressor Binding to Synthetic DNAs

of Defined Nucleotide Sequence. Proc. Natl. Acad. Sci. U.S.A. 69, 761 (1972).

26. Jayaram, B., Sharp, K. A. & Honig, B. The electrostatic potential of B-DNA. Biopolymers 28, 975–993 (1989).

CHAPTER II

Uniaxial and Dynamic Electrostatic Confinement of Nanoparticles

2.1 Introduction and background

Uniaxial confinement methodology confines nanoscale entities in solution along a single axis (1D) without the use of geometrical barriers. Interactions between colloidal particles and structured surfaces have been exploited in various confinement and manipulation studies (as mentioned in chapter I) that rely primarily on fluid flow or geometric barriers. Confinement of single molecules has been achieved using electro-kinetic feedback guided by tracking of a fluorescent label, but photo physical constraints limit the trap stiffness and lifetime[1]. Krishnan et. al demonstrated the geometry induced trapping of nanometric objects in fluidic slits but the system relies primarily on charged geometric barriers[2]. While many of these methods incorporate indirect methods of confining nanoparticles, actively controlled, direct charge-field interactions between charged entities are more versatile and can be tailored to specific

applications. Some shortcomings of existing techniques have been discussed in the table below.

Confinement techniques	Pros	Cons
Di-electrophoresis	• Uncharged particles can be trapped • Both AC and DC voltages can be used • No double layer effects in aq. solvents • No polarization effects and no electrolysis	• Highly charged particles cannot be trapped • Requires non-uniform electric fields • Only positive or negative dielectrophoresis • Particle should be large1-100um
Optical Tweezers	• Used in biological systems • Uncharged particles can be trapped • Damage-free manipulation • Suited for sensitive force measurements • Many buffer solutions can be used	• Small forces (pico-newtons) • Complex and expensive setup • Particles have to be sufficiently polarizable • Lack of selectivity, versatility • Low throughput
Geometrical, Electrokinetic traps (ABEL,PAUL)	• Non invasive particle manipulation • Charged particles can be studied • Independent of mass and dielectric function	• Photo-physical constraints • Low throughput • Not flexible • Suited for one system and one particle

Figure 2.1: Various confinement techniques and their advantages and shortcomings

In this chapter, we show that by actively tuning the surface potential of a one-dimensional nanoline structure; we can uniaxially confine nanoparticles without the usage of geometric barriers. We demonstrate this by using metallic line-charges in conjunction with charged nanoparticles that are trapped independent of their mass and dielectric function. The confined entities are free to diffuse uniaxially and their behavior can be studied using various particle motion monitoring methods[3]. The stiffness and stability of our electrostatic confinement methodology is easily tuned by adjusting the electrostatic potential of the charged lines and the ionic strength of the solution, lending itself to integration with other manipulation methodologies. We

envisage that these features will not only complement current particle motion-monitoring studies but also work as a platform for wide-ranging applications in the patterning, assembly, and manipulation of nanometric objects[4].

2.2 Diffusion and Brownian motion of nanoparticles in solution

Nanoparticle suspensions differ from solutions in that the substance used as a solute is appreciably larger than the solute of a solution. A phenomenon known as Brownian motion keeps the particles suspended in the solvent[5]. Brownian motion is the constant bombardment of the colloid particles by the solvent molecules in a solution at equilibrium. This action prevents the colloid particles from settling out of the solvent. More importantly, Brownian motion contributes to the diffusion of colloid particles through the solution. In 1905, Albert Einstein investigated this phenomenon and derived a general expression for the diffusivity of colloid particles in solvents[6]. If we observe such a particle for a time interval t, we will see it displaced by a position vector r. Repeating this over, we can calculate the average displacement during time interval t, and but no other forces like gravity or hydrodynamic flow should act, we should find that the average uncorrelated $< r > = 0$, which means that there is no preferred direction for the random forces exerted by the water molecules

on our nanoparticle. Therefore, we characterize Brownian motion not by the average displacement over some time, by instead by the average displacement-squared[7]:

(1) Three dimensional: $< |r|^2 > = 6\ D\ t$

(2) One dimensional: $< |r|^2 > = 2\ D\ t$

Where, D is called the diffusion constant or diffusivity (cm^2/s) of the particle. The diffusion constant D depends both on the size and shape of the particle, and on the viscosity and temperature of the fluid that it is moving through. In our experimental system, we rely on both the 3-D and 1-D (uniaxial) diffusion as the change in diffusivity from indirectly confirms the uniaxial confinement of nanoparticles in solution. This is covered in the later section on particle movement analysis.

2.3 Confinement mechanism for charged nanoparticles

Charged nanoparticles in a fluid can be confined on a landscape of electrostatic traps structured onto a surface[8,9]. Particles undergoing Brownian motion in a suspension, when introduced onto these surfaces fall into local electrostatic potential wells[10], remaining trapped in them as per the relation $\exp(\Delta F_e/k_BT)$, where the electrostatic potential energy F_e is a function of the spatial location of the particle, k_BT is the thermal energy at temperature T, and k_B is the Boltzmann constant. We utilize this

ratio to overcome the thermal motion of nanoparticles in the vicinity of a charged surface. Our experimental setup is based on creating a tunable, spatially modulated electrostatic potential profile near a metallic (Au) line-charge by biasing it against a counter electrode, in an ionic solution. The setup consists of a microfluidic channel sandwiched between two fluidic electrodes that acquire an opposite charge when they are biased using an external DC voltage source (Figure 1.3). One surface consists of a nanoline pattern topographically structured by nanofabrication techniques (Figure 2.2). Transparent conductive (ITO) substrates were used as the counter electrode as they allow for optical access to the interior of the fluidic cell.

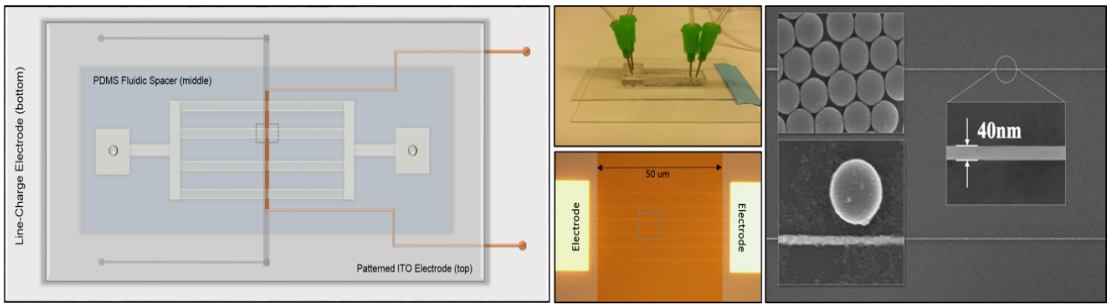

Figure 2.2a: Experimental of the fluidic cell schematic (left). Gold 1-D Line electrodes (middle). SEM and micrograph of a 40nm nanoline and nanoparticles made using e-beam lithography

Charged nanoparticles dispersed in an ionic solution (10^{-4}M) acts as the dielectric medium between the two electrodes. Imprinted and ion etched PDMS films (100um) act as spacers in our fluidic cells. The 1-D line charge pattern is realized by

fabricating a metallic nanowire (~35-50 nm) whose surface potential as well as polarity can be dynamically controlled at will by an applied potential bias. These 1-D nanoline electrodes have a geometric as well as an electrostatic significance when they interact with nanoparticles. Higher ratio of particle size to that of the line charge enables for sharper electrostatic potential wells. In our experimental system, these structures help with reducing non-specific binding events and creating a 1-D electrostatic potential favoring uniaxial confinement. Although, large area electrodes have been shown to assemble[11] an ensemble of nanoparticles for various applications, they inhibit motion, reversibility and single particle interaction characteristics that our system illustrates.

2.4 Materials and methods

2.4.1 Device Fabrication

All cover slips were cleaned using standard protocols and stored in ethanol. The bottom cover slip served as the counter electrode and was sputter coated with a 70nm Indium Tin Oxide (ITO) layer. The thin ITO layer provided for electrical connectivity and was transparent enough so that we could acquire good quality microscopy images from across the electrode. The top cover slip, which served as the working electrode,

was patterned with nanostructured 1-D Au metal lines. For the metal line pattern, hard Si molds were made using e-beam lithography and then they were replicated on cover slips using nanoimprint lithography. PDMS spacers (h=100um) were sandwiched between these two coverslip electrodes, creating a microfluidic cell with the ITO/PMMA layer facing up and the patterned metal lines facing down. The volume of the channel was kept constant at $0.5mm^3$ and the solution, and charged polystyrene particles was introduced using capillary forces. The device was allowed to equilibrate for two hours before the experiments and was then sealed using uv-curable epoxy. Care was taken to avoid any air pockets or bubbles from nucleating inside the cell. Solution conductivity was measured to be 3.39 μS/cm which corresponded to a Debye length of ~27nm. The ζ- potential of the PS nanoparticles, under the experimental conditions, was measured to be -58.6 ± 7 mV. The particles were imaged using an inverted fluorescence microscope (Nikon eclipse TE-2000-U). A schematic of the device is shown in Figure 2.3. The device was placed on the microscope stage with the ITO electrode facing downwards and a 100X oil immersion objective (N.A. 1.4) was used to image the particles kinetics from across the transparent electrode. A Gaussian filter was used to identify the centroids (PSF) of the particles, using the fluorescent intensity signal[12].

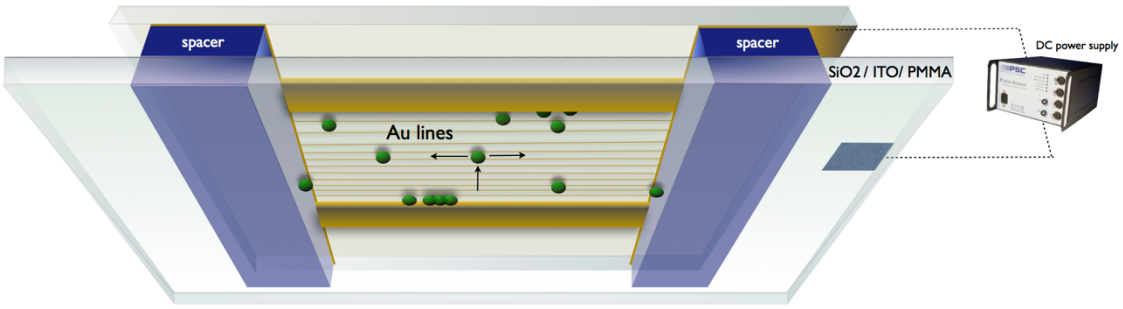

Figure 2.2b: Device schematic setup for uniaxial confinement with 50nm Au 1-D line electrode

Control devices were used to characterize the particle density, fluorescent signal, and the Brownian motion in solution. Electrical connections were made to the electrodes by attaching copper wires (d~0.5mm), using an Indium paste. A DC potentiostat (RSR DC-HY5003) was used to apply potential across the electrodes. The ITO electrode was given a negative polarity with respect to the metallic nanoline electrode.

2.4.2 Nanoparticle Characterization:

Charged, fluorescent, latex particles (40nm-500nm, diameter) serve as the test objects in this current study. Not only are these particles monodisperse in size but also demonstrate a signal to noise ratio (SNR) that is suitable for particle tracking with a localization precision of 10's of nanometers. For our experiments, a 0.2% suspension

was made by aliquoting particles in a 0.1mM monovalent salt solution. They are also negatively charged in solution (-COOH) (-0.83e/nm^2), making them favorable for studying electrostatic interactions. The ζ-potential of the colloids at the conditions of the experiments was measured to be –56.4 ± 6 mV, the Debye length ($\lambda_D = \kappa^{-1}$) was found to be ~30 nm from a conductivity measurement of the system (3.45 μS/cm). Representative fluorescence micrographs obtained in-situ are shown for far field of views of 180umx180um (Figure 2.5) and for interactions between 40nm line-charges and 500nm latex particles (unless otherwise mentioned). Spherical, fluorescent, charged, polystyrene nanoparticles carried a negative charge in solution, due to the high concentration of carboxylate groups (−COOH ⇄ COO− + H+) on the surface. The particles had an exceptionally intense fluorescence (505/515nm) with 106 fluorescein equivalents per nanoparticle and were compatible with our microscope.

2.5 Results

2.5.1 Confinement characteristics for charged nanoparticles

In solution, the electrostatic potential near a charged surface decays exponentially in an ionic solution, characterized by Debye length (L_d). An oppositely charged nanoparticle will experience an electrostatic attraction in the vicinity (3~5 L_d) of the

charged line[13]. The surface charge of the lines coupled with the charge of the particles, generates an electrostatic interaction in the vicinity of the line-charge. As the particles in the bulk of the solution undergo free Brownian motion, it is only when they approach the electrode through pure thermal diffusion that they feel the electrostatic interaction. In lieu of this, we ran 1-D FEM simulations for calculating the volumetric size of the cell and the particle density required. Considering a cylindrical coordinate system with boundary conditions fixed at $300L_d$ we release particles at various positions (L_d) and calculate the probability of these particles to interact with the charged line electrode (see supplementary information). Figure 2.6 correlates this scenario at various driving voltages. The effective range of interaction, outside of which the particles undergo pure Brownian motion, determines particle confinement. Based on our simulation, a particle density of 10ul/ml, length of line charges l >100um is fitting for confining 10 particles in 9.2 seconds. The distance between the electrodes was not considered as the number of particles per unit volume was kept constant. This number can be linearly extrapolated by adding more number. of line charges to the system (as seen in our experiment) or by increasing the particle density. A small volume (~10 μL) of the colloidal suspension at a particle density of

3.1 x 10^{11} (particles/ml) was placed between the parallel planar electrodes held at a separation of 100um with an ion etched, thin film PDMS spacer.

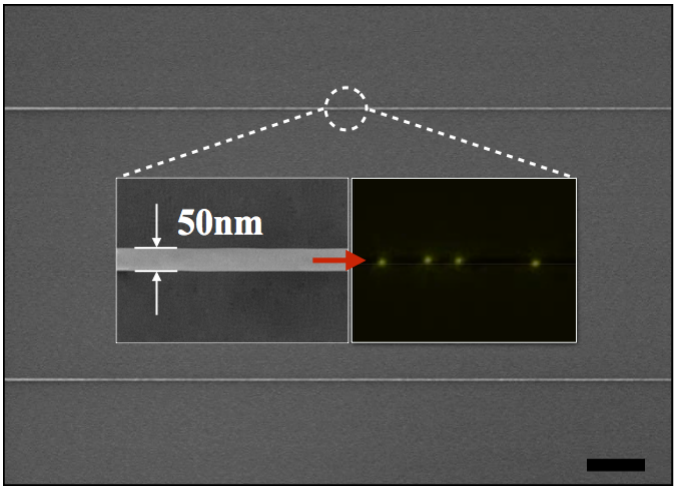

Figure 2.3: SEM image of 1D nanoline structure and a fluorescence micrograph of 100nm particles confined to the nanoline on application of a DC voltage (inset)

The cross-sectional area available for assembly was 0.8 mm^2. The device was mounted on the stage of an epifluorescent microscope for in-situ visualization with a numerical aperture, NA = 1.4 oil immersion objective. A potentiostat applied a constant DC voltage (0-4V) and measured the resultant current densities. All samples were allowed to equilibrate for 30mins before imaging. It is important to emphasize that the low voltage electric field does not overcome thermal motion of the particle, but rather provide a driving force towards denser configurations of nanoparticles near

the electrodes. This is evident in the micrographs in Figure 2.4, which shows particle aggregation near the electrodes at various applied voltages.

2.5.2 Observation of 1D Line-particle interaction

Application of a voltage bias across the two electrodes produces a radial 1-D potential well around the line-charge. Charged particles that are in the vicinity are electrostatically attracted and migrate towards the line charge, and are subsequently confined by the potential energy well, which then undergo localized diffusion uniaxially along the line-charge. The magnitude of the voltage and ionic strength of the solution control the magnitude and range of the attractive force. It was observed (as seen in Figure 2.4), only particles close to the line charge feel the electrostatic interaction and attracted to the line and exhibit random diffusion along the 1-D line charge, the rest remain unaffected by the line and undergo free Brownian motion in solution. Reducing the voltage bias on the charged line liberates the particles back into the solution. Reversing the polarity of the applied bias on the line-charge, hastens the particle desorption process, as the force changes from attractive to repulsive. Careful examination of image stacks show that the interaction comprises of three distinctive phases: a) Electrostatic confinement of the nanoparticle to the line charge.

b) One-dimensional diffusion of the nanoparticle along the line charge. c) Desorption of particles on charge polarity reversal. The transient densification of the particles was seen after t > 60s near the line electrodes by imaging at 30fps. Images that characterize the kinetics of particle migration are shown in Figure 2.6. During the first phase at lower voltages, the particles remained in the bulk of the solution, undergoing random thermal diffusion. As the voltage is ramped in steps of 0.1V, particle migration towards the line electrodes commences. For t > 2mins; 0.8V < V < 1.2 V; the particles continued to densify over time. Even though densification occurred in this time period, the particles remained highly mobile due to Brownian translations at this voltage and volume fraction. This behavior is a direct consequence of the voltage induced electrostatic interaction energy (F_e) overcoming the thermal energy of the particles ($F_e > k_bT$). Figure 2.6 shows the effect of different applied voltages on the particles. The samples were imaged at the line-charge after at least 10mins. This time was sufficient for the system to reach a quasi-steady state structure configuration. This was visualized as the particles came into the focal plane, which was set at the line electrode in our microscopy experiment. Particle distance in the z-direction was characterized by their fluorescent halo, which grows larger as the particles move further from the focal plane. Here, the time it takes for the all particles

to be confined on the line electrodes has not been considered, as it was apparent that for a sufficiently long time interval, all the particles would eventually land on the electrodes. This has been simulated to be on the order of days for the volume fraction used in our experiments. For t > 2mins; 1.2 < V < 1.5 (intermediate voltage), particles exhibit confinement and 1-D diffusion over the line-charge. Figure 2.4 shows that at applied voltages greater than 1.5 V results in a much denser colloidal phase at the electrode surface than that observed for the lower applied voltages, with some aligned particle domains. However, the particles further above the electrode are more disordered and diffuse. Further increment in voltage (>1.8V) lead to the particles residing on the electrodes without exhibiting any free diffusive motion. At 3V, the nanoparticles appeared jammed, with limited mobility due to the rapid densification caused by the high initial driving currents. We consider this point to be the higher threshold for our test objects. Although our test particles are monodispersed and uniformly charged, it should be noted that in our experiments some particles show anomalous behavior which can be attributed to the discrepancy in size and charge on the particles. By reducing the voltage bias to 0V, it was seen that the particles are released from the line-charge and move back into the bulk solution. This shows that the particles are not permanently bound at the electrodes and are only localized near

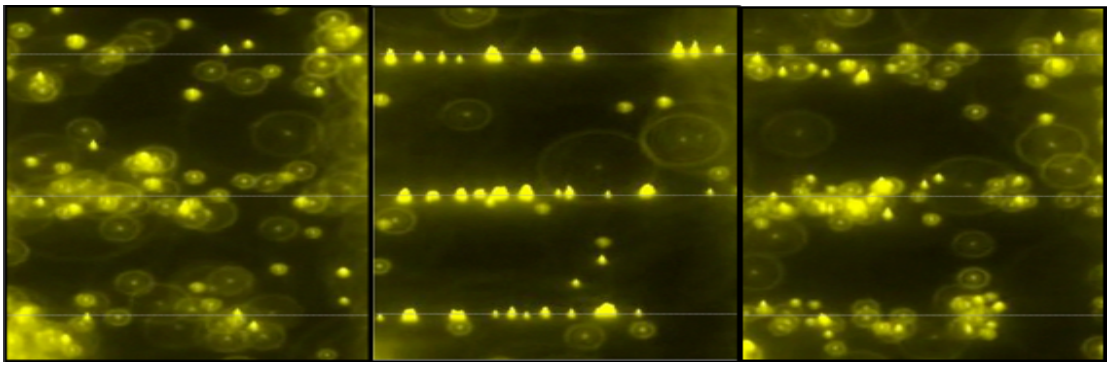

Figure 2.4: Three fluorescence micrographs representing: electrostatic attraction, confinement and reversibility

the electrode. Reversing the polarity of charge on the electrodes hastened the de-trapping process as interaction force changes from attractive to repulsive. This behavior was confirmed for 500nm, 100nm, and 40nm particle diameters. Thus, variation of the applied voltage results in a series of reversible transitions between the line-charge and particles. Lower applied voltages (<1.2 V) lead to uniaxial diffused-confinement of particles over the line-charge. At intermediate applied voltages, particles exhibit 1-D diffusion along the line-charge. Lastly, at large voltages (>2 V), a jammed, arrays of particles are observed near the electrode. The effective electric field in the solution between the electrodes can be calculated through direct measurement of the current density for all the conditions. In our hypothesis, the electric field generated between the electrodes has an effect on the colloidal particle motion only to the extent that it is dominant relative to Brownian motion of the

particles, producing denser configurations near the electrodes. Although, no significant differences in current were found using a 0.1vol% solution of particles, we believe that faradaic reactions do take place at the electrodes, as the setup was open to atmosphere. Experiments were conducted on 5 samples for 300 seconds each. At lower voltages the current generated was small (<0.2uA/cm2). At each applied voltage, the current progressively decreases over the duration of the experiment (t>200s).

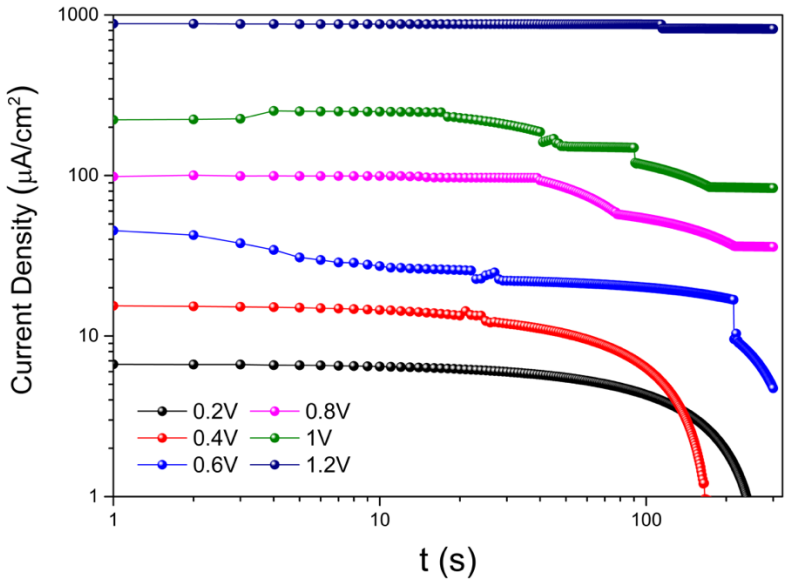

Figure 2.5: Current densities in our system and their degradation at various applied potentials

This is consistent with other studies that suggest that this behavior is due to mass transfer transients in the diffusion layer near the electrodes and depletion of

reactants in the bulk of solution (see Figure 2.5). Accordingly, even after long durations (t >700s) particles seem to diffuse towards the electrode. It is important to emphasize that the low voltage electric field does not overcome thermal motion of the particle, but rather provides a driving force towards denser configurations near the electrodes due to an initial driving current (ionic diffusion) that decays over time. As for most surface electrode reaction, current is a monotonically increasing function of the applied voltage.

Increasing the voltage bias beyond 2V caused the particles to stick permanently on the Au lines. Presumably, electrochemical reactions between the particles and the electrodes can cause these permanent-binding interactions. Based on experimental current density measurements, we see that there is some amount of faradaic currents at our operating voltage but these currents are caused due to the initial double layer charging events and reduces over time as the sample reaches a quasi-equilibrium state. It can be seen in that some of the particles are clumped together at certain points on the electrode and this occurred due to unavoidable fabrication defects that give rise to concentrated electric field “hotspots” on the line electrodes. Intuitively thinking, by patterning small perturbations at designated locations along the line, we would see the particles undergo diffusion along the lines

and eventually get confined at these perturbations under sufficiently strong voltage bias.

2.5.3 Analyses of particle movements

The spatial sampling of an electrostatic potential well by a particle strongly depends on the charge it carries and characteristics of the line-charge: the higher the charge on the particle, the greater the expected stiffness of its confinement, which manifests in the experiment as a smaller root mean square (r.m.s.) spatial displacement. Importantly, any increase or decrease in stiffness arising from particle charge would be expected to appear in 1-D spatial dimension. A scatter plot of the (r.m.s.) displacements of each particle convincingly demonstrates just this correlation, and presents a simple and rapid route to measure the diffusivity dispersion of a sample at the single particle level. As shown in Figure 2.6, a Gaussian fit to yields a trap stiffness of 0.047 pN nm^{-1} for a 500nm particle, in the direction orthogonal to the line charge. This value is comparable to optical traps used for other single particle monitoring studies [14]. The particle diffusion over the metal lines was characterized using the centroid determination method and the centroid of fluorescent particles in each image was determined by fitting a 2D fluorescence intensity profile to a

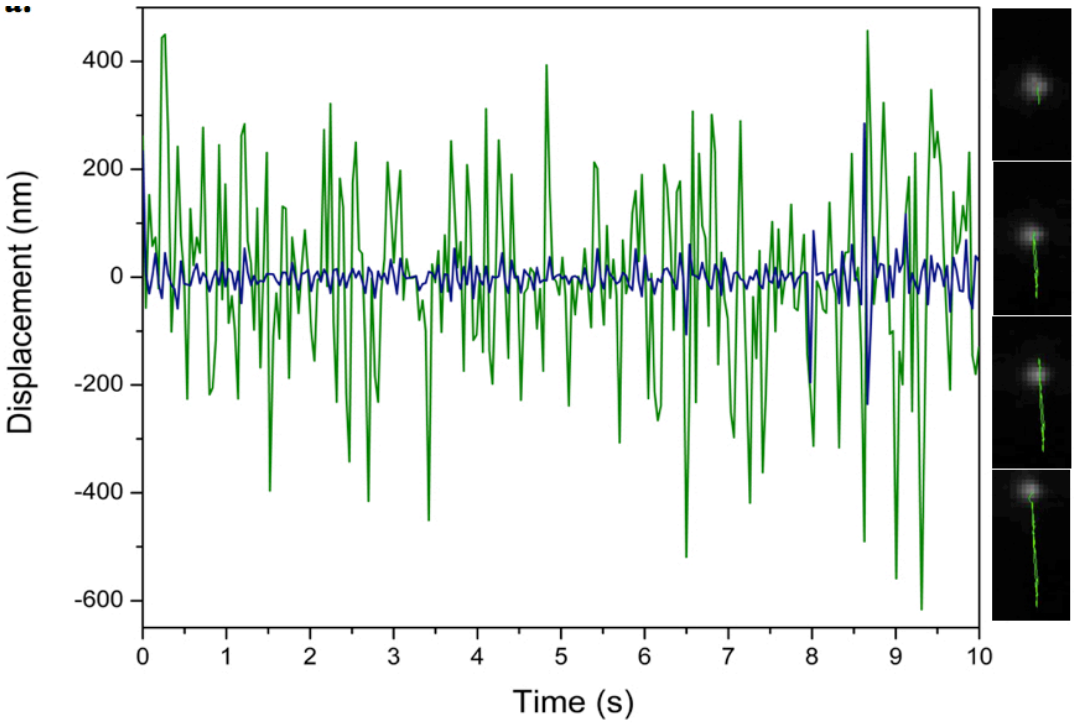

Figure 2.6: Particle trajectories (displacement of centroid) along (GREEN) and perpendicular (BLUE) to the line with respect to Time(sec). Right: shows snapshots of a single nanoparticle confined on the line charge and tracking its centroid during the diffusion process.

Gaussian. To show the 1-D diffusion of the particles along the line charge, we plot the particle centroid displacement along the nanoline and perpendicular to the line in Figure 2.6. Confinement of the particle to the charge line is very apparent. Particle tracking data shows a cumulative movement of 32um along the line-charge. This can be further established by quantifying the mean square displacement (MSD) data presented in Figure 2.7. We obtain the 1-D diffusion coefficient (D) by plotting the

MSD versus the time interval over which the displacement takes place. The MSD is calculated using:

$$MSD(i\Delta t) = \sum_{j=1}^{N-i} \frac{(x_{i+j} - x_j)^2}{N-i} + \frac{(y_{i+j} - y_j)^2}{N-i}$$

Where xi and yi denote centroid positions of the protein in the ith image, iΔt represents 'i'time steps each of duration Δt (=0.038 s), and N is the total number of positions measured[15].

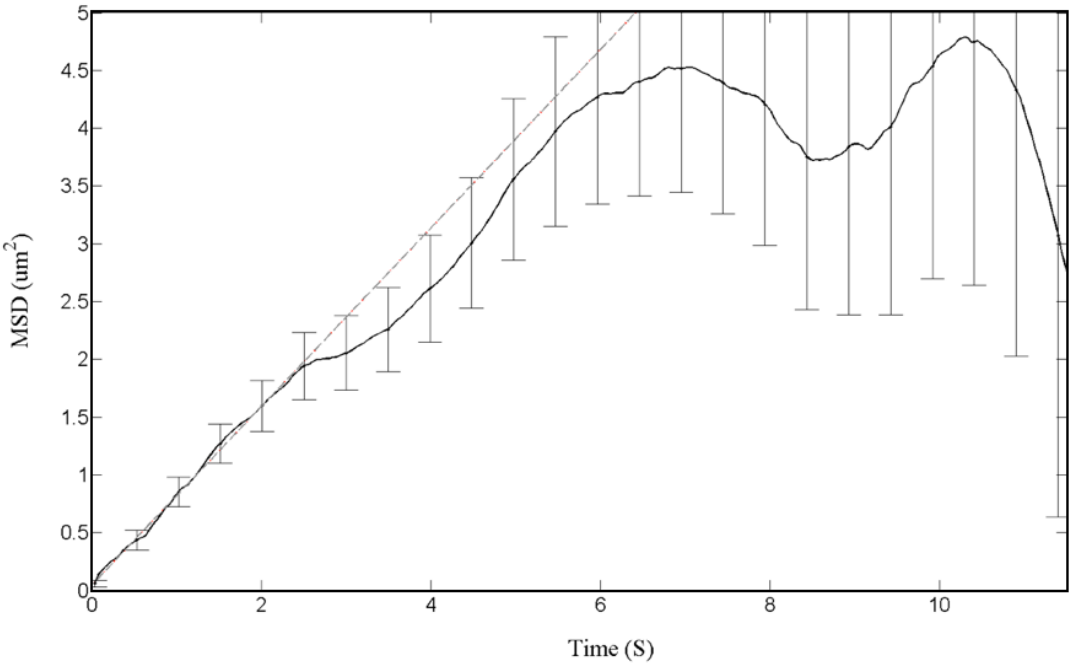

Figure 2.7: Mean Square Displacement data for particle diffusion on the line charge

Using the slope of the line projected by the first 60 time steps, the diffusion coefficient is thereby calculated to be 1.09 x 10^{-13} m^2/s for a 250nm (radius) particle

at [KCl] = 0.1mM. The Mean Square Displacement plot shows a typical diffusion behavior for a uniaxially confined particle, where the diffusion coefficient is of the same order as in bulk solution (~10^{13} m2/s). This clearly shows that the particle is undergoing free translational, uniaxial diffusion in one-dimension just as hypothesized. In addition to this, we characterize the change in diffusivity of the confined particles in relation to the applied voltage bias. Further study is underway to analyze this behavior as variation in particle surface charge density, size and shape can favorably change this behavior.

2.6 A model system for electrostatic binding interactions

When a charged nanoparticle approaches a line charge, the charge density is regulated with the help of charge redistribution. Net charges at the surface, however, are unchanged. As it is difficult to theoretically incorporate short-range forces, calculation of the line charge density, at an applied voltage, for the interaction between a charged particle and a charged line is a problem of considerable intricacy[16]. Theoretical progress has been made for these systems by the use of statistical mechanical theories such as Brownian dynamics simulation and mean-field descriptions [17]. We explain this behavior by investigating the effects of the

electrostatic potential on the colloidal suspension. To measure the net electrostatic potential energy for any given particle/line-charge interaction, we analyze the shape of the confining potential and compare this with a model calculation. We model the nanoline electrode as a cylindrical line charge with variable line charge density λ (C/m). Using cylindrical coordinates for a charged line (with a radius b_0 and charge density λ (C/m) and the ionic surrounding (with ionic screening strength, = $1/L_d$), the electrostatic potential created by a line when a particle is at a distance 'r' away from it can be obtained by solving the Poisson-Boltzmann equation: Solving this equation with typical boundary conditions, gives the screened electric potential generated by the charged line in the presence of surrounding ions:

$$\psi_{line}(r) = \frac{\lambda}{2\pi b_0 \varepsilon \varepsilon_0 \kappa} \frac{K_0(\kappa r)}{K_1(\kappa b_0)} \qquad r \geq b_0$$

Where K_0 (x) and K_1 (x) are the 0(1) order modified Bessel function of the second kind. Using this model, we qualitatively analyze how our system would behave when changing the radius of the charged line b_0, Debye length L_d, and the line charge density λ. The measured axial probability density distribution of particle displacement P(r) yields a spatially dependent potential via the Boltzmann relation. Using COMSOL Multiphysics, we calculate the spatial distribution of the electrostatic

potential in the trapping nanostructure by numerically solving the nonlinear Poisson–Boltzmann equation in one dimension. The system consists of a sphere of fixed surface charge density embedded in an electrolyte, which in turn is bounded by surfaces of a given charge density. Analytical parameters for the simulation were the wall charge density (boundary condition), ionic strength and size and surface charge density of the interacting test object. The background ionic strength of the electrolyte and an estimate of the wall charge density can be obtained from conductivity and zeta potential measurements, respectively. Thus, for a particle of a given diameter and charge, the line charge remains the only free parameter in the calculation. The free energy of the system as a function of particle position was calculated by summing the electrostatic field energies and entropies over all charges in the system. Figure 2.9 presents a series of axial free energy curves as a function of line surface potential for the conditions of the experiment. Increase of the line charge density by an applied voltage leads to an increase of the depth of the one-dimensional potential well (>700KbT); Increasing the Debye length by reducing ionic concentration not only increase the depth of the potential well but also enlarge the interaction region, Increase of the radius of the charged line also enlarges the interaction region but results in a quick decrease of the depth of the potential well. In our model, we

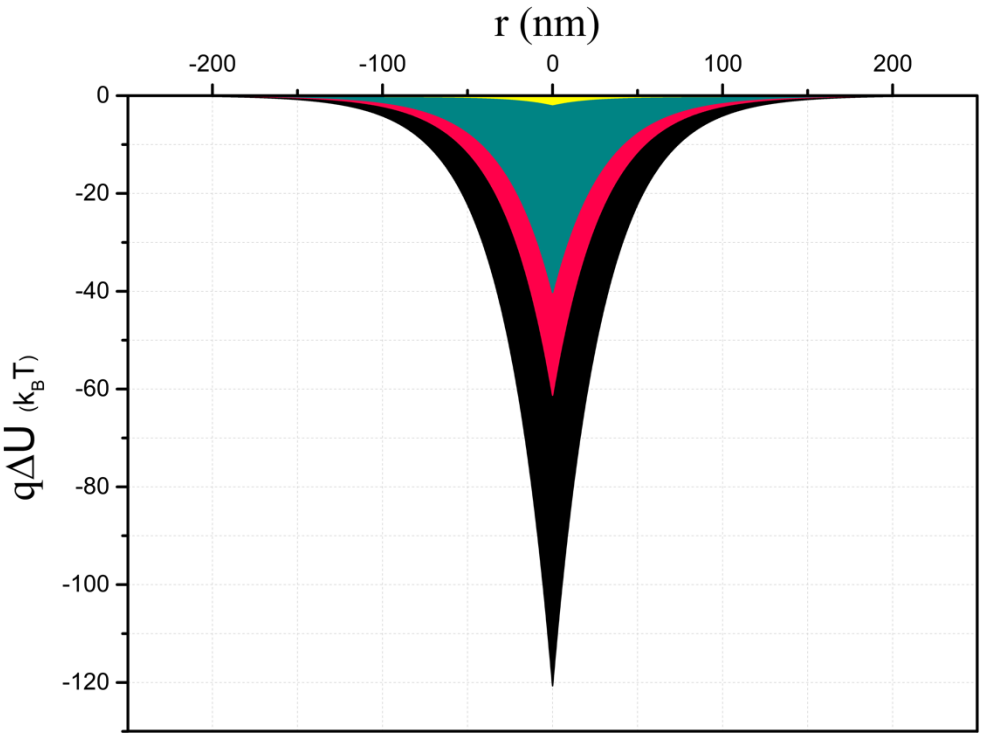

Figure 2.8: Variation in electrostatic potential energy, near a line charge. Potential for a nanoparticle (q~8850e⁻). (Black) b=35nm, C=0.1mM, λ=130.5e/nm (experimental condition). (Red) b=35nm, C=0.1mM, λ=43.5e/nm. (Cyan) b=35nm, C=0.2mM, λ=130.5e/nm. (yellow) b=140nm, C=0.1mM, λ=130.5e/nm.

consider the total charge to be centered at the centroid of the nanoparticle and so the distance of closest approach to the line is greater than the radius of the particle. While our preliminary calculations suggest that the polarization forces in the system are not large enough to overcome the Coulombic forces, they do contribute to the interaction. This model is a very good fit for describing electrostatic confinement of particles; but it can also be applied to electrostatic interactions at smaller length scales. This relies

on the fundamental question that ‘Is it possible to make two systems of different sizes and charge densities, comparable, or to be more precise, show similar dynamical properties?’ If the answer is yes, then our experimentation and theoretical analysis can shed light on the dynamics and transport properties of the much smaller interaction scales that are difficult to observe visually and thus provide for a framework applicable at different interaction length scales.

2.7 Discussion

Comparing our synthetic interaction with a biological interaction means that all the parameters (dependent or independent) that influence it should be scaled by the same factor. This can be accomplished by maintaining the same potential energy (U) for the two systems at geometrically similar positions. Scaling involves geometric parameters (particle radius, line charge radius, and Debye length) and electrical parameters (surface charge density of the particle and of the line). It should be noted that in our calculations, charge on the particle was assumed to be at the centroid of the particle, but in the case of protein the charge was centered at the surface. This is a good approximation for calculation purposes otherwise the protein would not be attracted to the DNA as the distance of closest approach would be greater than 3-5 L_d.

These observations based on our experimental and theoretical analysis are a good fit to emphasize how working with larger systems can help us understand the nuances of a smaller system. It depicts a scenario that allows one to zoom in on interactions occurring at a smaller length scales. Although short-range forces are not incorporated, the model is compatible, realistic and can be viewed as an idealized representation. In essence, by looking at realistically larger system combined with our experimental observations, it is possible to get some insight into the fundamental role that electrostatics can play in the process of transcription.

2.8 Conclusion and future outlook

We have used actively tuned, one-dimensional nanostructures to induce uniaxial confinement of charged nanoparticles in solution. We see a strong correlation between experimental and theoretically reported order parameters. While the experimental evidence on the behavior of charged nanoparticles near a line charge can be substantiated by our theoretical model, we envisage that this methodology and the results can fill in the gap that the recent theoretical studies have tried to justify. Moreover, it is a versatile method that requires only a small number of particles to study the kinetics of particle confinement and can be integrated easily with other

methods. It is also an excellent candidate for studying colloids such as Janus particles that are often only available in limited quantities. Due to the scope for programming and tuning the system described here, it provides flexibility to select particular kinetic pathways for confinement, assembly and fractionation of colloidal suspensions.

2.9 References

1. Cohen, A. E. & Moerner, W. E. The anti-Brownian electrophoretic trap (ABEL trap): fabrication and software. Biomedical … (2005). doi:10.1117/12.598689
2. Myers, C. J., Celebrano, M. & Krishnan, M. Information storage and retrieval in a single levitating colloidal particle. Nature Nanotech 10, 886–891 (2015).
3. Han, L. et al. in Mathematics of DNA Structure, Function and Interactions 150, 123–138 (Springer New York, 2009).
4. Trau, M., Saville, D. A. & Aksay, I. A. Assembly of colloidal crystals at electrode interfaces. Langmuir 13, 6375–6381 (1997).
5. Li, F., Josephson, D. P. & Stein, A. Colloidal Assembly: The Road from Particles to Colloidal Molecules and Crystals. Angew. Chem. Int. Ed. 50, 360–388 (2010).
6. Investigations on the Theory of the Brownian movement. (1956).
7. Michalet, X. Mean square displacement analysis of single-particle trajectories with localization error: Brownian motion in an isotropic medium. Phys. Rev. E 82, 041914 (2010).
8. Nanoscale Electrostatic Trap for Charged Particles. 1–20 (2012).
9. Lin, T., Rubinstein, S. M., Korchev, A. & Weitz, D. A. Pattern Formation of Charged Particles in an Electric Field. Langmuir 30, 12119–12123 (2014).
10. Amin-Patel, A. P. Microfluidic device integration of electrostatic corral

trapping systems. ProQuest Dissertations and Theses; Thesis (M.S.)--The University of Wisconsin - Milwaukee, 2014; Publication Number: AAT 1567717; ISBN: 9781321287066; Source: Masters Abstracts International, Volume: 54-01.; 91 p. (2014).

11. Dziomkina, N. V. & Vancso, G. J. Colloidal crystal assembly on topologically patterned templates. Soft Matter 1, 265–15 (2005).
12. Parthasarathy, R. Rapid, accurate particle tracking by calculation of radial symmetry centers. Nature methods (2012).
13. Ammam, M. Electrophoretic deposition under modulated electric fields: a review. RSC Adv. 2, 7633–14 (2012).
14. Stafford, G. C., Jr., Kelley, P. E., Syka, J. E. P., Reynolds, W. E. & Todd, J. F. J. Recent improvements in and analytical applications of advanced ion trap technology. International Journal of Mass Spectrometry and Ion Processes 60, 85–98 (1984).
15. Charsooghi, M. A., Akhlaghi, E. A., Tavaddod, S. & Khalesifard, H. R. A MATLAB program to calculate translational and rotational diffusion coefficients of a single particle. Computer Physics Communications 182, 400–408 (2011).
16. Kashyap, H. K., Annapureddy, H. V. R., Raineri, F. O. & Margulis, C. J. How is charge transport different in ionic liquids and electrolyte solutions? J. Phys. Chem. B 115, 13212–13221 (2011).
17. Kontturi, K., Murtomäki, L. & Manzanares, J. A. Ionic Transport Processes: in Electrochemistry and Membrane Science. (OUP Oxford, 2008). doi:10.1093/acprof: oso/9780199533817.001.0001

CHAPTER III

Size-Selective and Spatial Confinement of Nanoparticles on Dynamically Nanoinscribed Void Patterns

3.1 Introduction and background

Templated self-assembly (e.g., chemically modified surfaces and patterned topography) [1-3] with fundamental electrostatic forces expand on the ability to direct particle confinement with controlled interparticle spacing and non-close-packed structures[4]. We demonstrate a simple low-cost methodology to selectively confine 500nm nanoparticles by using a 2D dynamically nanoinscribed (DNI) sinusoidal void pattern on a flexible polymeric substrate. In the methodology proposed here, discrete nanoparticles are arranged selectively on structured surfaces using directed electrostatic assembly. In contrast to conventional self-assembly, directed assembly does not merely fill the nanostructured array with randomly dispersed nanoparticles in solution, but selectively arranges nanoparticles of a certain size at positions that are defined by the substrates' nanostructured geometry and charge regulation in the EDL.

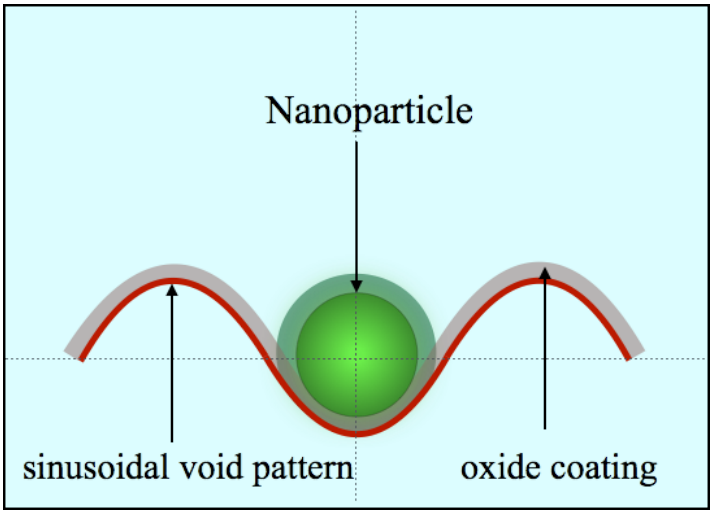

Figure 3.1: Schematic depiction of our void confinement framework

Fundamental electrostatic interactions guide this confinement into arrays but we also experimentally demonstrate how the extent of the electrical double layer (EDL) overlap between the interacting species plays a key role and depends closely on the relative dimensions of the nanoparticles as well as the pattern geometry.

3.2 Current methodologies for structured confinement of nanoparticles

Selective assembly of particles of a certain size in the form of a colloidal array can benefit many other applications including photonic band gap crystals, nanoelectronic devices, optical switches and filters, filtration devices and biological assays[5-9]. A prerequisite for these applications using particles ensembles as functional entities is often control and selectivity of their arrangement on a surface[10,11]. Doing so

with standard microfabrication techniques is difficult, and it is often time consuming and inefficient to create sparse patterns of small nanoparticles using subtractive top-down processing. We present a highly parallelizable means of patterning and sorting nanoparticles in a size-selective manner onto substrates based on the double layer interaction between nanoparticles and a 2D sinusoidal void patterns[12]. Size-selective particle confinement, separation and sorting entails particulate matter of a variety of shapes and sizes are confined based on the physical attributes of the individual particles.

A number of methods have been reported for size selective particle confinement, sorting and patterning, including electrophoretic deposition (EPD)[13], flow-induced packing into cavities of controlled dimensions, deposition by the Langmuir-Blodgett (LB) technique[14], deposition by gravitational sedimentation, and evaporation of particle suspensions. Pick-and-place robotic manipulation has been demonstrated for micro particles and might be possible for nanoparticles[10], but is difficult and requires handling every particle individually. Scalability in today's devices renders such serial fabrication techniques economically unrealistic. Self-assembly methodologies emerge either from particle-particle interactions, which limit the achievable particle arrangements to certain dense packing but with no selectivity,

or from particle-substrate interactions, which allow greater control of the final particle positions. Chemical or topographical patterning of the substrate is usually necessary to obtain selectivity and high-throughput processing[15]. Moreover, most self-assembly processes lack size-selectivity and are based on suspensions, incurring all the contamination problems of wet processing. These shortcomings have so far prevented self-assembly from becoming a viable option in applications like filtration and bio-sensing[16]. Therefore, a suitable low-cost, low-complexity, method must be developed. In particular, in-plane two-dimensional (2D) patterns are more favorable for integration into the thin-film structures and device fabrications. From a biological standpoint, as most biological molecules carry a charge when dispersed in an ionic solution, we envisage that this methodology could also be used for the trapping and sorting of cancer cells from other blood constituents[17]. Neither functional modifications nor complex enrichment processes are required. Various groups are looking for better ways to find circulating tumor cells (CTC) and their efforts fall essentially into two categories. The first approach is biochemical and involves trapping the cells using antibodies that bond to them. The second approach is mechanical, with the strategy of filtering out the CTCs. Both of these methods have drawbacks. Antibodies can only bond to the cells if they can get close enough, and

although circulating tumor cells are bigger than red blood cells, they are about the same size as white blood cells so filters have limited success. Currently, isolation of CTCs from peripheral blood is performed using antibody-based anti-EpCAM capture[18]. While this technique can detect epithelial cells, it misses poorly differentiated cells or those that have undergone epithelial-to-mesenchymal transition (EMT), which is a hallmark of metastatic disease. Commercial systems like DEP array and Fluidigm also suffer from high- throughput and imaging constraints. Therefore, a more sensitive and reliable method that enables researchers to isolate all varieties of CTCs in a label-free fashion from cancer patients' blood samples is a vital next step. We envisage that this methodology, when coupled with CTC applications could be this next step as it requires less preparation, has high throughput, is label-free, and is capable of capturing various types of CTCs.

3.3 Material & Methods

3.3.1 Sinusoidal void patterning methodology

Flexible substrates films like PF, PC and PET were pre-cleaned before patterning. Details of DNI processes along with mold preparation and cleaving

procedure can be found elsewhere. All polymer substrates (PET and PC from Tekra Corp.) were used as purchased and cleaned using IPA followed by nitrogen drying before the patterning process. For Performing DNI, we prepare a well-cleaved SiO_2 mold containing the desired pattern along the edge then bring the mold edge in contact with the substrate at a proper angle and then slide the mold edge over the substrate with conformal contact being maintained. This process is subsequently done in orthogonal directions (2D-DNI) to produce the sinusoidal void pattern as shown in Figure. DNI uses the sharp edge of a hard grating mold to inscribe the pattern over the substrate. The mold edge can be locally heated to control the degree of plastic deformation of the substrate at contact, thereby tailoring the resulting pattern geometry. 2D patterning via DNI is easily accomplished by performing two 1D DNI processes in series along orthogonal (or any oblique) directions (denoted as 2D-DNI hereafter). Figure shows the SEM images of 2D nanopatterns fabricated by 2D-DNI. Here the first DNI-patterned grating can be slightly deformed by the second DNI patterning since DNI relies on conformal contact throughout the inscribing stroke. However, since the mold openings do not touch the patterned surface during the second DNI, the overall void patterns clearly emerge. In DNI, the pattern period is

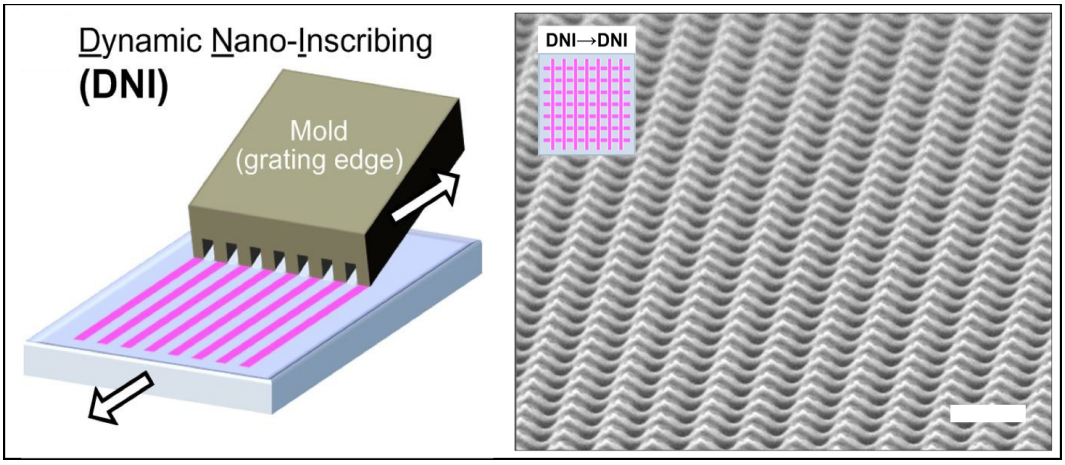

Figure 3.2 Dynamic nanoinscribing (DNI) schematic and methodology(Left). 2D-DNI performed on polycarbonate substrate creating a sinusoidal void pattern with dimensions:400nmx400nmx800nm (right). Scale bar is 1um.

dictated by that of the grating mold and voids of various sizes and geometry can be inscribed in a facile manner with high throughput. For instance, we use a 700 nm period SiO_2 mold for patterning in this work (unless otherwise noted in this work). These void patterns are precisely inscribed to a certain size, which has a direct relationship to the particle size. Furthermore, the morphologies of the sinusoidal voids created by 2D-DNI can be specifically tailored by changing the substrate material, applied force, and processing temperature increasing its selectivity behavior.

3.3.2 Device fabrication for in-situ visualization

Our experimental device (Figure 3.7) consists of a microfluidic cell chamber made

out of two transparent cover slips. One of these cover slips contains the 2D array of 2D-DNI- patterned 700nm pitched voids coated with 10 nm thick Al2O3 oxide layer which is positively charged when immersed in an ionic solution. The other acts as a

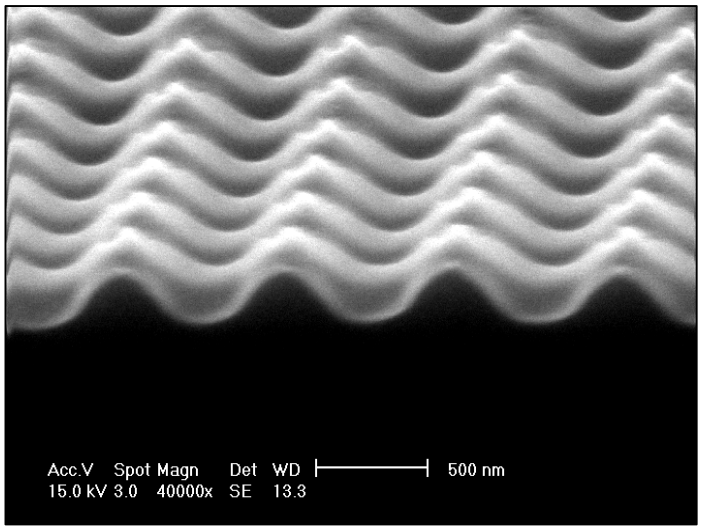

Figure 3.3: SEM images of 2D-DNI sinusoidal void pattern formation

transparent medium for top-down microscopic characterization. For the nanoparticle confinement cell fabrication, a 2D-DNI-patterned PC substrate was coated with a 10 nm-thick Al_2O_3 layer by RF sputtering (Lab 18-2, Kurt J. Lesker) and was bonded to a pre-cleaned glass cover slide. The two cover slips are held at a separation of 1 mm by etched poly-dimethyl siloxane (PDMS) spacers that are bonded to the coverslips by activating their surfaces using an oxygen plasma treatment. This cell was heated at 80C for 2 hours to get rid of any trapped air bubbles in the PDMS and was checked

for leakage. Care was taken to ensure there was enough distance between the void patterned substrate and the top coverslip so that particle concentration gradients do not appreciably affect the device. Perforated holes in the cover slips acted as inlets and outlets with tygon tubing inserted and the whole chamber is sealed using a uv-curable epoxy. Fluorescent labelled (FITC-515nm) polystyrene nanoparticles were purchased from Molecular Probes Ltd., centrifuged and re-alliquoted into solutions with varying ionic concentrations. This nanoparticle suspension at an initial volume fraction of 0.1 % wt. was injected into the chamber at a fixed flow rate (10ul/min) if not noted otherwise in this work. The ionic solution containing NPs was allowed to equilibrate inside the chamber for 15 minutes and the complete device was then attached to a holding structure on the microscope stage for visualization.

3.3.3 Microscopic Characterization

Electron Microscopy was performed using a Philips XL30-FEG at the typical operating voltage of 5-25 kV. Solution conductivity and nanoparticle measurements were quantified using commercial DLS light scattering instrumentation (Zetasizer Nano, Malvern Instruments). For Fluorescence microscopy, we used an Olympus BX-100 to gather frames at various time intervals. Exposure times of 10ms, 30ms and

100ms were used to visualize the movement of particles in solution. As the particles were coated with FITC dye molecules, a 485 nm excitation light source was used to illuminate the sample. The experimental microscopy setup is shown in the figure below.

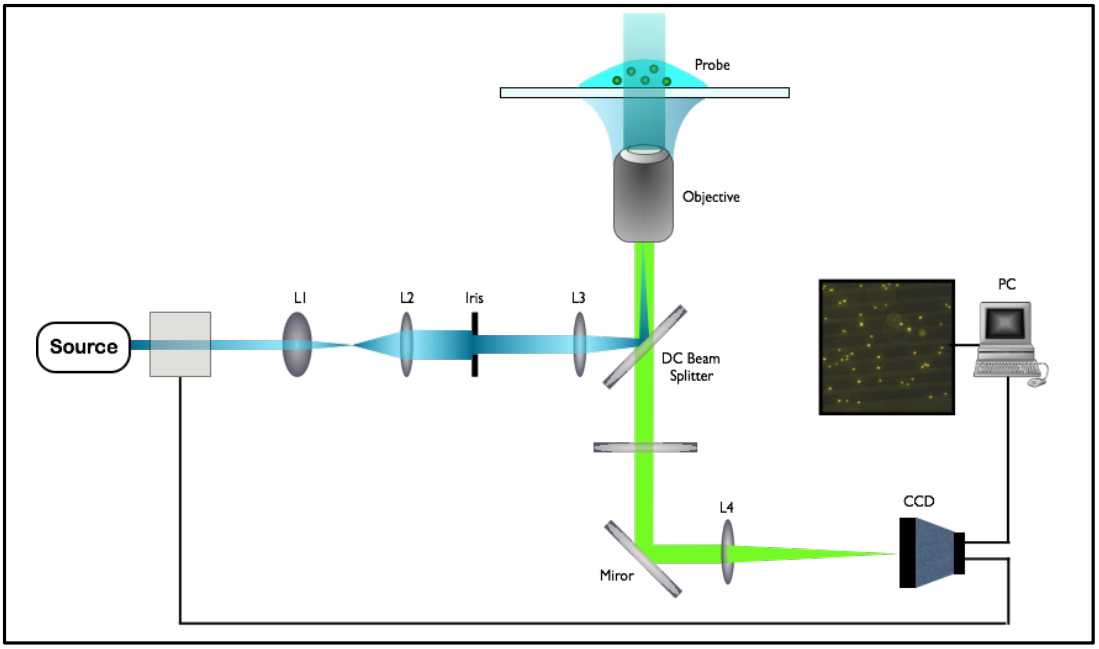

Figure 3.4: Fluorescence microscopy setup for in-situ visualization

3.3.4 Surface charging mechanism of oxides and charge density

The value of the zeta potential for the slit surfaces was estimated from electro-osmotic flow measurements in fluidic slits[19]. For the oxide coated void patterns, the electrostatic potential distribution was theoretically estimated by solving the Poisson-Boltzmann equation using constant-charge boundary conditions and verifying overall

electroneutrality of the system. Experimental surface charge density deviated from theoretical results due to three dimensional structuring of the surface. Metallic oxides form surface charges in the presence of ionic solution through dissolution and subsequent adsorption of hydroxyl ions in solution. Alumina surfaces immersed in an ionic solution acquire a positive surface charge density primarily through the dissociation of terminal -OH groups (see below){Ntalikwa:2007tz}. The degree of dissociation and thus the surface charge density results from an equilibrium between counter ions at the surface and free ions in the bulk electrolyte:

$$\text{Al-OH} + \text{H}^+ \longrightarrow \text{Al}^+\text{OH}_2 \qquad \text{pH} < 7.0$$

$$\text{Al-OH} \longrightarrow \text{AlO}^- + \text{H}^+ \qquad \text{pH} < 8.2$$

$$\text{Al-OH} + \text{OH}^- \longrightarrow \text{AlO}^-\text{OH}_2 \qquad \text{pH} > 8.2$$

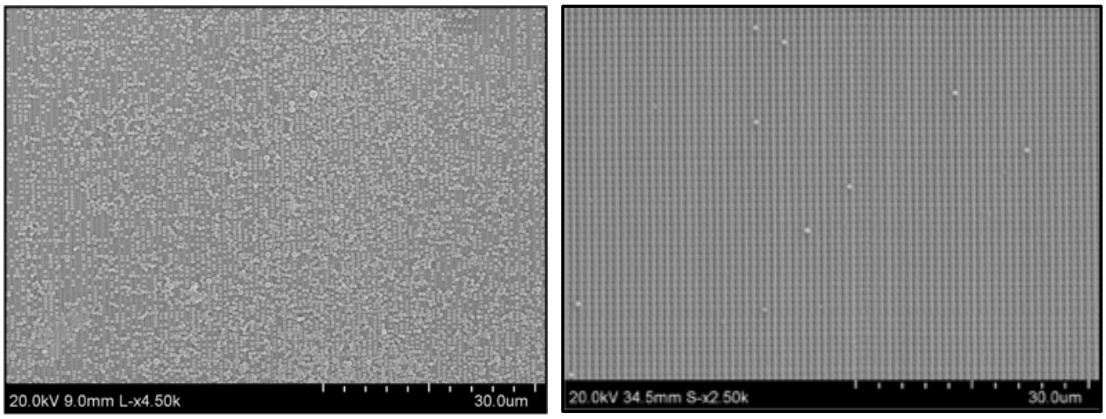

Figure 3.5 Confinement in patterned voids coated with oxide(left). Minimal confinement visible on patterned voids without oxide

This behavior and the polarity is highly dependent on the pH of the interacting solution. Electroosmotic flow experiments were performed to quantify and estimate

the surface charge density of our void pattern. As seen in Figure 3.6, for an sputter coated Al2O3 film the surface charge density is positive at neutral pH and can be tuned by changing the pH of the solution. Control experiments confirm that particle confinement ceases at pH > 8 and at ionic concentration < 10^{-6} [M]. The charging behavior and capacity of Al_2O_3 films in solution have been extensively studied in the past and it should be noted that the surface charge density of Al_2O_3 films degrade overtime in ambient conditions caused by the above mentioned reactions.

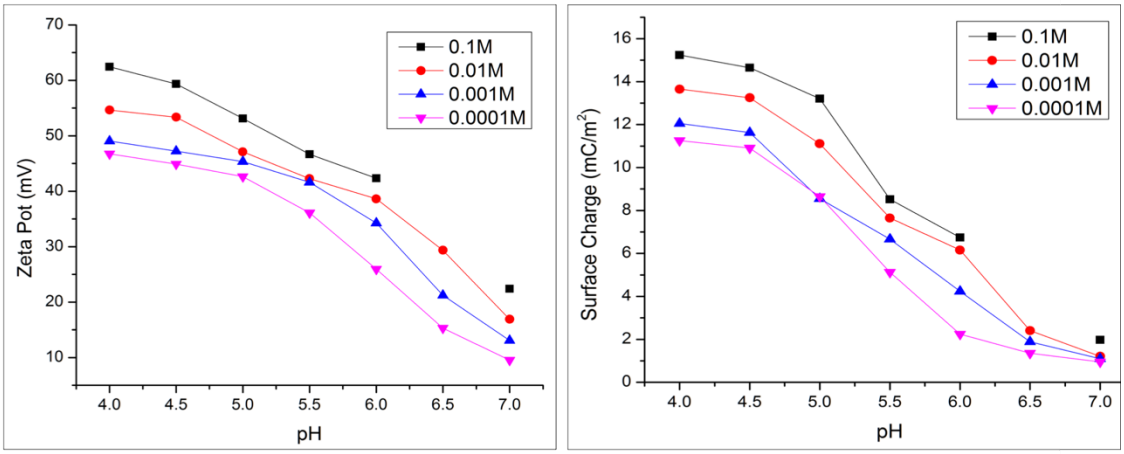

Figure 3.6: Zeta Potential and electroosmotic surface charge density estimations at various pH and ionic concentrations for 10nm Al_2O_3 sputtered coating

Conformity of the coating was confirmed using an SEM. The deduced surface charge densities are in relatively good agreement with other research groups that experimented with similar volumetric structures. Furthermore, various other oxides like CaO, NiO and MgO can also be used to vary the polarity and degree of charging

at the desired operating pH.

3.5 Mechanism and methodology of particle confinement

Colloidal particles assemble into arrays whose order depends closely on the relative dimensions of the spheres and the pattern as well as the pattern geometry. In the methodology proposed here, discrete nanoparticles are arranged on structured surfaces using directed electrostatic assembly which relies on charge regulation in the overlapping EDL's. In contrast to conventional self-assembly, directed assembly does not merely fill predefined structures with randomly dispersed nanoparticles in solution, but arranges nanoparticles at positions that are defined by the substrate's nanostructured geometry and surface charge. This is accomplished by creating a nanostructured 2D sinusoidal void pattern on a polymer substrate using the dynamic nanoinscribing technique (DNI) (as seen in Figure 3.3). A sputter coated oxide layer provides this void pattern with a surface charge and when exposed to an ionic solution containing charged nanoparticles of opposite charge polarity, spatial confinement is initiated. Our process is based on generating a sinusoidal electrostatic potential on the 2D-DNI-patterned substrate that has the ability to couple with oppositely charged nanoparticles in an ionic solution (10^{-3}M). Most macromolecules

as well as many oxide surfaces develop a net electric charge (by either the dissociation of chemical groups or the adsorption of ions from solution) when suspended in an ionic solution. The charged NPs undergoing Brownian motion in solution experiences an electrostatic attraction in the vicinity of the oppositely charged surface. As the suspension of negatively charged polystyrene NPs (−1.8e nm^{-2}) flows into the fluidic cell, their size and surface charge density control the trapping behavior. We can directly visualize the instantaneous confinement and assembly of fluorescently labelled 500 nm diameter polystyrene particles in the

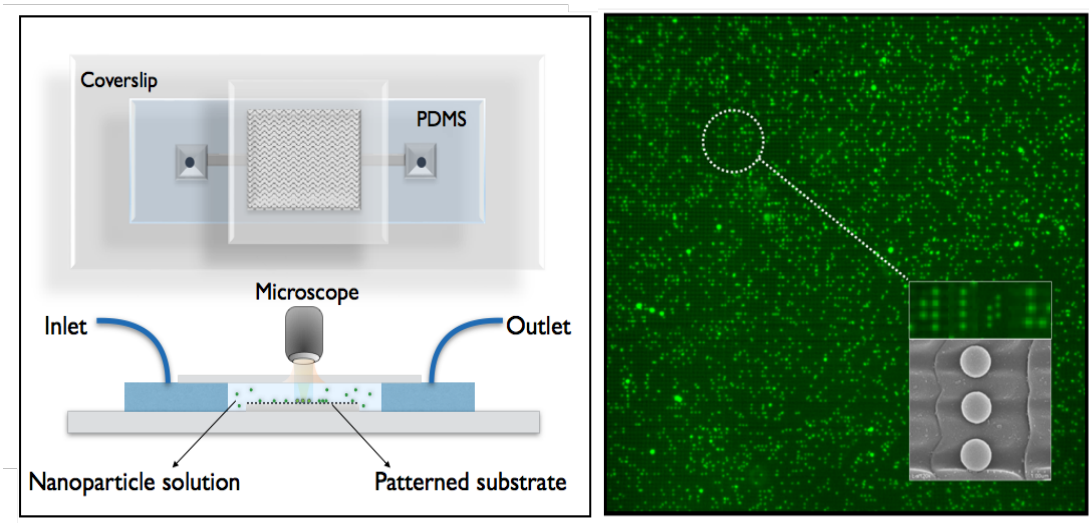

Figure 3.7: Experimental fluidic cell chamber schematic(left) Epi-fluorescent micrograph of 500nm diameter particles confined into patterned voids(right).

patterned voids (Figure 3.7). The 2D sinusoidal potential profile accentuates the trapping process, enabling the size specificity of this confinement methodology. A

schematic, shown in Figure 3.7, depicts the experimental setup. Using a combination of electrostatic interactions in ionic solutions and our 2D patterning technique, we have created a single-step methodology to selectively confine and pattern the nanoparticles on flexible substrates. We present experimental and theoretical evidence to better understand this selective interaction and confinement characteristics. In the absence of Al_2O_3 layer, the nanoparticles diffuse freely within the chamber and are homogeneously distributed, as shown in Figure 3.7. In the presence of the oxide layer, particles in the vicinity of a voids are packed and confined onto the substrate; however, a small subpopulation of particles remains diffused as they do not 'sense' any electrostatic attraction created by the oxide layer. Nanoparticle confinement is initiated due to the electrostatic interaction between the negatively charged nanoparticles and the positively charged alumina void pattern and their double layer overlap. As seen in Figure 3.7, it was confirmed that the particles were confined inside the voids as the symmetric patterns were visibly identified in the fluorescence micrograph. The well-defined patterns contain a distribution of particles along adjacent voids and are periodically spaced. As this process is diffusion limited and no external stimuli is applied, increasing the particle concentration increases the fill ratio to a certain degree and further increasing the particle concentration beyond

0.8wt% did not appreciably increase the fill ratio. The fill ratio is relatively low and this can be explained due to the incongruity between the relative size differences between the nanostructured voids and the nanoparticles. Our understanding so far is that this could arise due to three factors. (1) The 2D-DNI is a mechanical process so no two voids are similar in dimensions (2) Relative size variation in commercially available nanoparticle samples was experimentally confirmed and (3) Particles that are already confined on the surface have a tendency to electrostatically repel particles in their vicinity (EDL). All these three factors substantiate the low fill factor and also accentuate the applicability of this methodology to confine particles or contaminants of varying sizes. Confined particles adhere to the surface strongly as no amount of rinsing the channel with DI water helped in detaching these particles. Using physical force like placing the substrate in an ultrasonic bath dislodged most of the particles from the surface.

3.6 Understanding the size-selective nature of nanovoid pattern

The above mentioned experimental results are intuitively from a fundamental electrostatic standpoint and this interaction between 500nm particles and a similarly sized void could be expected but an equally interesting occurrence would be that a

nanoparticle less than 500nm in diameter could also be trapped in these voids. To test this idea, we experimented with a fixed void size and tested three different particle sizes (200nm, 500nm, 1000nm) to see if the confinement was size-selective in nature. Under similar conditions and at the same mentioned flow rate we found that only particles of diameter ~500nm diameter were confined in the voids. In the case of 200nm particles some non-specific adsorption was observed but no appreciable confinement in the voids. Similar results were obtained when testing 1um particles. To understand this counterintuitive size-selective behavior, we simulated this interaction using the cosmos-multiphysics package and Finite element analysis. The sinusoidal void surface (400nm x 400nm x 800nm) was modeled with a volumetric equation. The electrostatic potential energy of this interaction is calculated by simulating this interaction as the particle enters the void in the z-direction, it can be seen that from a purely electrostatic standpoint, there exists a large energetic barrier to entry just before the particle enters the void and this is counterintuitively largest for the experimentally trapped 500nm particles and only the 200nm particles should be trapped in the voids. There is another aspect to this interaction that needs to be considered and its the charge regulation in the overlapping double layers.

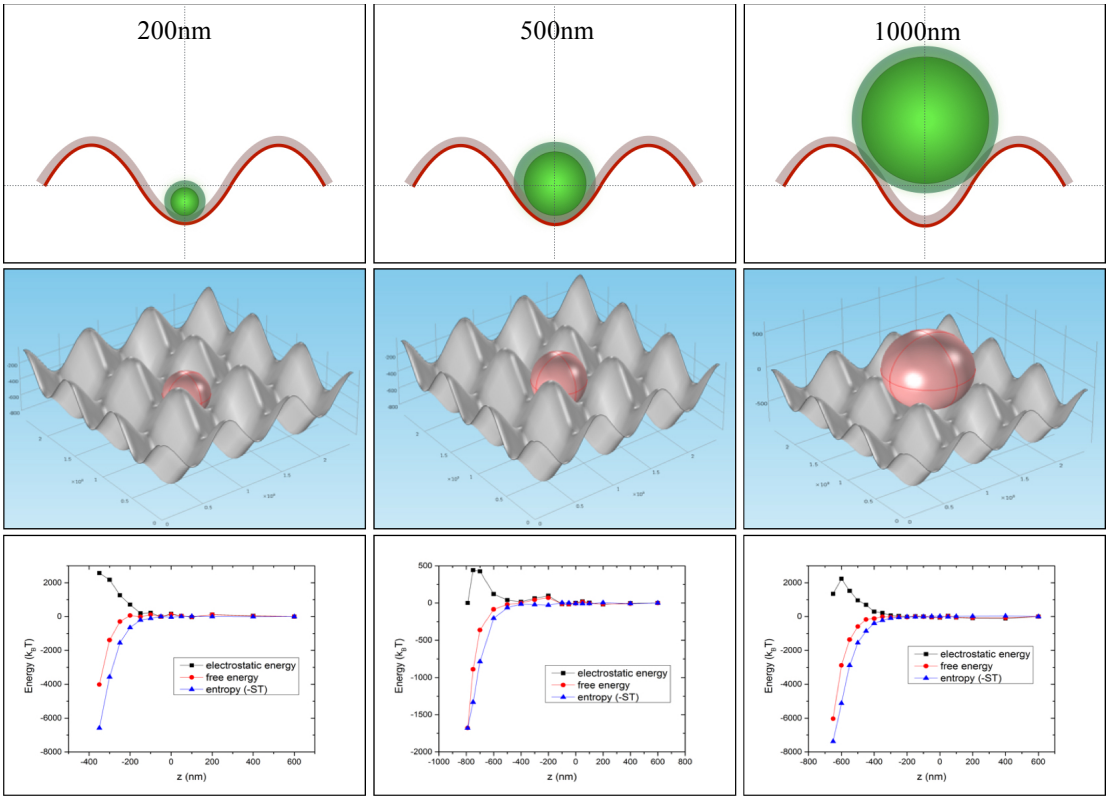

Figure 3.8: Top: Extent of EDl overlap for 100nm, 500nm and 1000nm particles. Middle: Sinusoidal void pattern model with particle position at z = 0. Bottom: Plotting the electrostatic, entropic and free energy of the interaction as charge regulation takes place.

The charged nanoparticles and the oxide coated void surfaces have an equal and oppositely charged Debye length in the ionic solution, so as the individual double-layer overlap charge regulation or neutralization occurs and this plays a key role in the overall free energy of the interaction as shown in Figure 3.8. The extent of double layer overlap dictates the interaction in the short range and the electrostatic interaction dictates the confinement of the particles in the relatively long range. The

overall interaction energy is most complimentary in the case of 500-600nm particle diameter. by fixing the void size, only particles of a specific diameter are confined and intuitively DNI can be used to vary the void pattern so that particles of varying diameter can be confined in a single step process.

3.7 Conclusion and future outlook

In summary, we have presented the facile, cost-effective, and easily scalable manufacturing of 2D micro/nano-patterns by creatively applying the continuous 1D grating fabrication techniques such as DNI multiple directions. Among many potential applications, we have demonstrated the use of such fabricated 2D patterns for the colloidal nanoparticle confinement, which could potentially lead to the sorting and trapping of various biological species including bacteria and circulating tumor cells. The excellent fabrication throughput of our method will facilitate the use of multi-dimensional micro/nano-patterns in many applications that require large areas.

3.8 References

1. Rycenga, M., Camargo, P. H. C. & Xia, Y. Template-assisted self-assembly: a versatile approach to complex micro- and nanostructures. Soft Matter 5, 1129–1136 (2009).
2. Gates, B. D., Xu, Q., Stewart, M., Ryan, D. & Willson, C. G. New approaches to nanofabrication: molding, printing, and other techniques. Chemical … (2005). doi:10.1021/"
3. Yin, Y., Lu, Y., Gates, B. & Xia, Y. Template-Assisted Self-Assembly: A Practical Route to Complex Aggregates of Monodispersed Colloids with Well-Defined Sizes, Shapes, and Structures. J. Am. Chem. Soc. 123, 8718–8729 (2001).
4. Kraus, T. et al. Closing the gap between self-assembly and microsystems using self-assembly, transfer, and integration of particles. Advanced Materials 17, 2438–+ (2005).
5. Kanamori, Y., Shimono, M. & Hane, K. Fabrication of Transmission Color Filters Using Silicon Subwavelength Gratings on Quartz Substrates. Photonics Technology Letters, IEEE 18, 2126–2128 (2006).
6. Velev, O. D. & Gupta, S. Materials Fabricated by Micro- and Nanoparticle Assembly - The Challenging Path from Science to Engineering. Advanced Materials 21, 1897–1905 (2009).
7. Ting, C.-J., Chang, F.-Y., Chen, C.-F. & Chou, C. P. Fabrication of an antireflective polymer optical film with subwavelength structures using a roll-to-roll micro-replication process. J. Micromech. Microeng. 18, 075001 (2008).
8. Möller, S. & Forrest, S. R. Improved light out-coupling in organic light emitting diodes employing ordered microlens arrays. Journal of Applied Physics 91, 3324–3327 (2002).
9. Green, N. G., Morgan, H. & Milner, J. J. Manipulation and trapping of sub-micron bioparticles using dielectrophoresis. Journal of Biochemical and

Biophysical Methods 35, 89–102 (1997).

10. Kraus, T. et al. Nanoparticle printing with single-particle resolution. Nature Nanotech 2, 570–576 (2007).
11. Righini, M., Zelenina, A. S., Girard, C. & Quidant, R. Parallel and selective trapping in a patterned plasmonic landscape. Nature Physics 3, 477–480 (2007).
12. Ok, J. G., Panday, A., Lee, T. & Jay Guo, L. Continuous fabrication of scalable 2-dimensional (2D) micro- and nanostructures by sequential 1D mechanical patterning processes. Nanoscale 6, 14636–14642 (2014).
13. Fukada, Y., Nagarajan, N., Mekky, W. & Bao, Y. Electrophoretic deposition—mechanisms, myths and materials. Journal of Materials Science 39, 787–801 (2004).
14. Guo, Q., Arnoux, C. & Palmer, R. E. Guided Assembly of Colloidal Particles on Patterned Substrates. Langmuir 17, 7150–7155 (2001).
15. Li, F., Josephson, D. P. & Stein, A. Colloidal Assembly: The Road from Particles to Colloidal Molecules and Crystals. Angew. Chem. Int. Ed. 50, 360–388 (2010).
16. Gopinath, S. C. B. Biosensing applications of surface plasmon resonance-based Biacore technology. Sensors & Actuators: B. Chemical 150, 722–733 (2010).
17. Sollier, E. et al. Size-selective collection of circulating tumor cells using Vortex technology. Lab Chip 14, 63–77 (2014).
18. Chiou, P. Y., Ohta, A. T. & Wu, M. C. Massively parallel manipulation of single cells and microparticles using optical images. Nature 436, 370–372 (2005).
19. Dependence of the Electroosmotic Flow in Bare Fused-Silica Capillaries from pH, Ionic Strength and Composition of Electrolyte Solutions Tailored for Protein Capillary Zone Electrophoresis. 1–10 (2003). doi:10.1365/s10337-003-0098-3

20. Ntalikwa, J. W. Determination of surface charge density of alpha-alumina by acid-base titration. Bulletin of the Chemical Society of Ethiopia 21, 117–128 (2007).

CHAPTER IV

Structured Coloring of Capped Nanoparticles for Optical Sizing

1.1 Introduction

Particle size dictates its surface area and influences many properties of particulate materials and coatings [1,2]. The size and shape of nanoparticles critically influences its light scattering properties[3]. Nanoparticles have unique properties in materials, as they help reduce volume and increase specific surface area[4]. Properties, such as band gap engineering of nanoparticles by quantum confinement have been investigated by researchers in various fields[5]. For these and many other reasons it is important to measure and control the particle size distribution and identify the relative size distributions of nanoparticles in an ensemble. By this we imply that if even monodisperse samples have relative size differences among particles that measure to be tens of nanometers as seen in Figure 4.1. Separation steps such as screening, and filtration may be monitored by measuring particle size before and after the process. Various methods have been devised to statistically measure the size distribution of

nanoparticles[6] but apart from electron microscopy, there are no high throughput methods to visualize the relative size distribution in a given sample of nanoparticles. Here we present a methodology to structurally color low-index nanoparticles based on their size.

4.1.1 Particle sizing and relative size distribution

A spherical particle can be described using a single number and that is the diameter because its identical in every dimension. Thus, many techniques make the useful and convenient assumption that every particle is a sphere[7]. These reproduce a normal size distribution for a given sample of nanoparticles. This statistical distribution is characterized by the standard deviation, mean and mode of the particle size. The reported value is typically an equivalent spherical diameter. This is essentially taking the physical measured value (i.e. scattered light, settling rate) and determining the size of the sphere that could produce the data[8]. Although this approach is simplistic and not perfectly accurate, the shapes of particles generated by most experimental processes are such that there is a size distribution associated for a given sample of nanoparticles as shown in Figure 4.1 which depicts a size distribution of monodisperse particles. As can be seen in this sample size there are a lot of particles

that are not 110nm in size and relative size of particles differ by as much as 30-40nm. (pre-characterized particles were obtained from https://nanocomposix.com/ collections/silica/products/100-nm-silica-nanospheres) This variation is particle size is what our methodology helps detect and characterize.

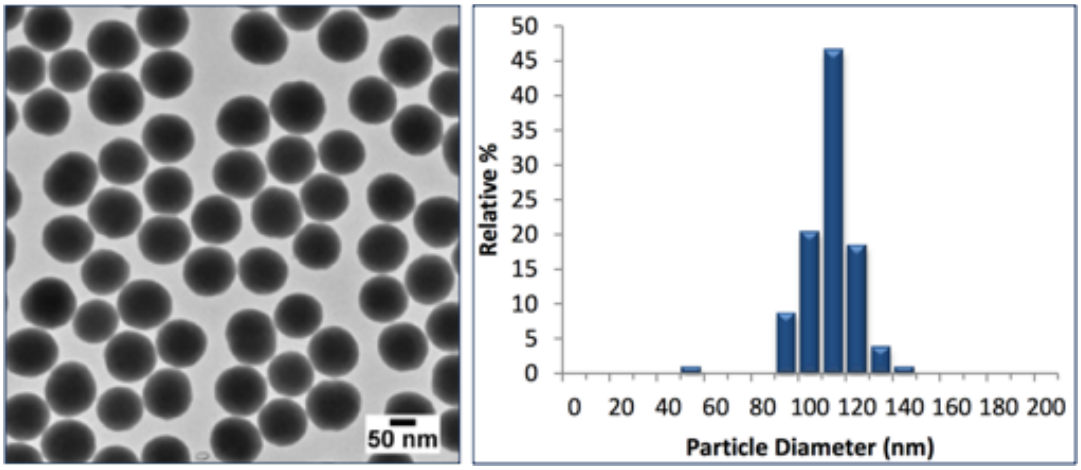

Figure 4.1: SEM micrograph of 110nm silica particles (left). Statistical size distribution of standard monodisperse 110 nm silica particles(right)

The most accurate techniques that can describe particle size using multiple values are microscopy or automated image analysis. Also in many light scattering methodologies used to characterize the particle size, the hydrodynamic diameter is represented which is different from the actual particle diameter[9]. When reporting a particle size distribution, the most common format used even for image analysis systems is equivalent spherical diameter on the x-axis and percent on the y-axis.

4.1.2 Methods for optical sizing of nanoparticles

Existing particle size characterization tools based on several principles including laser diffraction, dynamic light scattering and image analysis[10]. Each of these techniques generates results in both similar and unique ways. Most techniques can describe results using standard statistical calculations such as the mean and standard deviation. But commonly accepted practices for describing results have evolved for each technique. All particle size analysis instruments provide the ability to measure and report the particle size distribution of the sample. There are very few applications where a single value or a relative value is represented visually. Almost all real world samples exist as a distribution but in a research experiment where size uniformity of nanoparticles is important (chapter III represents one such case) it is crucial to know the relative size variation in a given distribution, especially where surface area is critical. There are several methods that exist and Figure 4.2 depicts the various methods that are currently used and they are listed in terms of their costs, complexity and size.

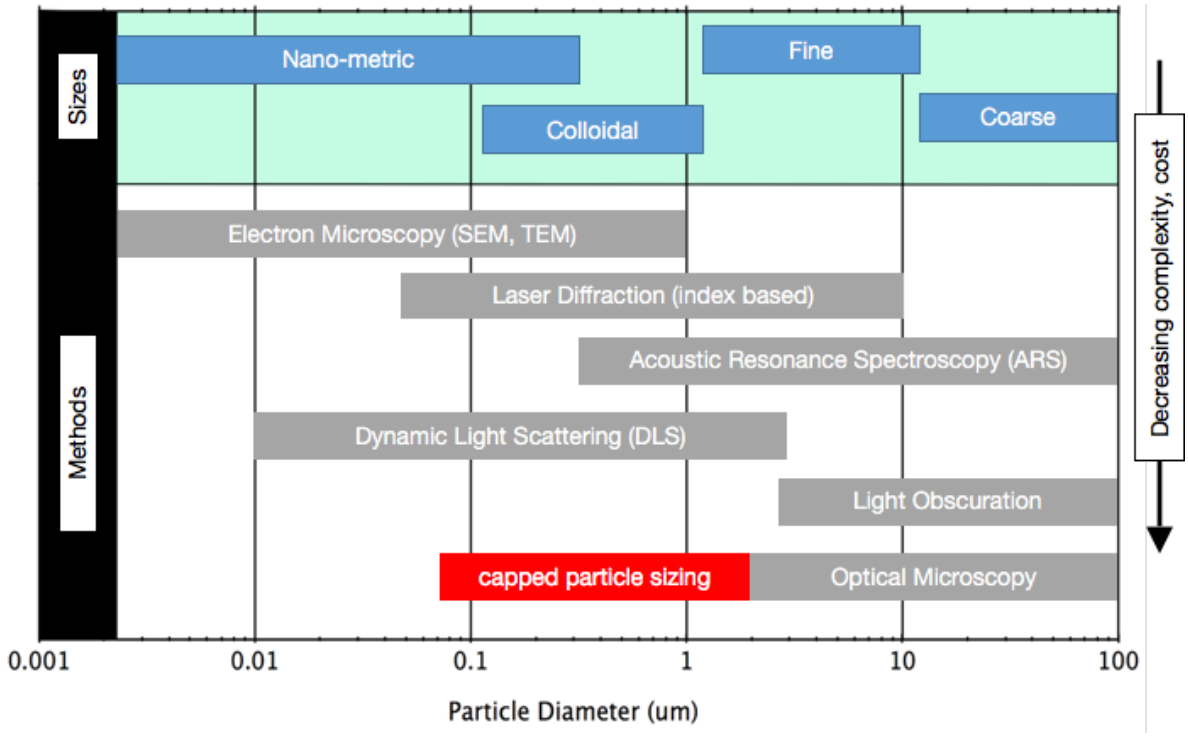

Figure 4.2: Most common methods used for particle sizing

As can be seen, the most widely used and the least complex and accessible method is optical microscopy with scanning electron microscopy on the other end of the spectrum. But optical microscopy is not very useful for measuring the particle diameters below ~2um in size[11]. We intend on expanding this predominantly used method to measure particle sizes below from 200nm to 700nm.

4.2 Capped nanoparticle optical sizing methodology

Our methodology for measuring relative variations on particle ensemble is based on

structurally coloring particles based on their size. This is accomplished by depositing a thin layer of metal on top of nanoparticles. Low-index nanoparticles like silica with a diameter of 500nm are dispersed onto a transparent substrate coated with a 70nm thick layer of Au. A second PVD deposition of 30nm is done on top of the particles as seen in Figure 4.4. This forms an aperture below the particle and a cap that whose size and

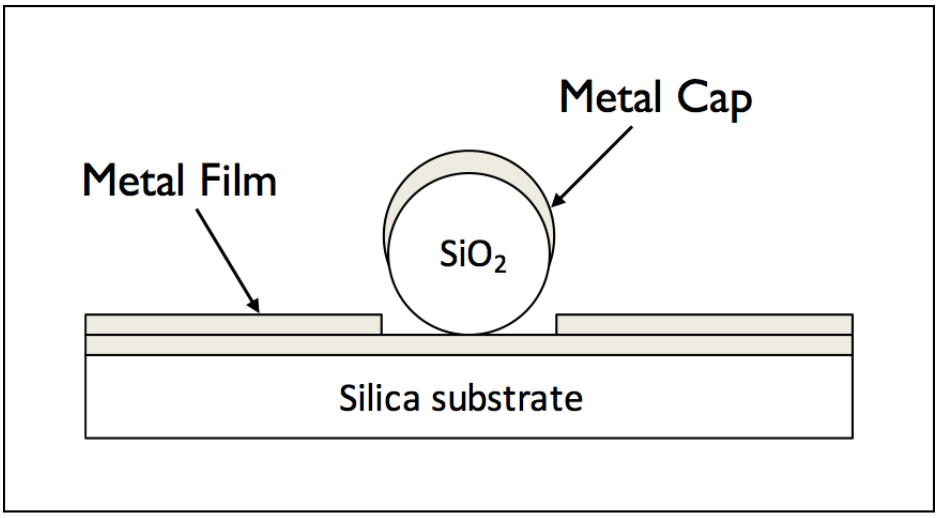

Figure 4.3: Schematic representation of the capped particle optical sizing methodology

dimensions are dictated by the diameter of the particles. Plasmonic cavity resonance characterized by a magnetic dipole[12] is localized between the cap and the bottom metal layer. When a light is passed through this aperture its gets localized inside this cavity and resonates at frequencies that are different for different cavity sizes (peak

shift). Small variations in the diameter of the particles change the distance between the metal cap and bottom metallic layer and this changes the resonant frequencies of the cavity which in turn gives of colors of different wavelengths.

4.2.1 Mie-scattering of capped nanoparticles

Many different theories could be applied to describe the optical properties of small particles based on their size[13,14]. A single particle is a light scattering object, for example for a silica particle commonly used for many applications the incident light excites free electrons on their surface which leads to an induced secondary electromagnetic flow on the surface of particles (plasmons) based on the Maxwell's equations[15,16]. Low-index particles absorb light as they scatter it. Sum of the absorption and scattering of a nanoparticle is termed as extinction. Mie theory[17] is one of the fundamental theories used in predicting the optical properties of spherical nanoparticles and if we looked at the extinction of silica particle and compared it with a silica particle with a thin Au shell (Figure 4.5), we see the appearance of resonant frequencies that can measured using a spectrometer and this optical spectrum is closely related to the size of the nanoparticle and so simulation results can inform us about expectations of various color frequencies.

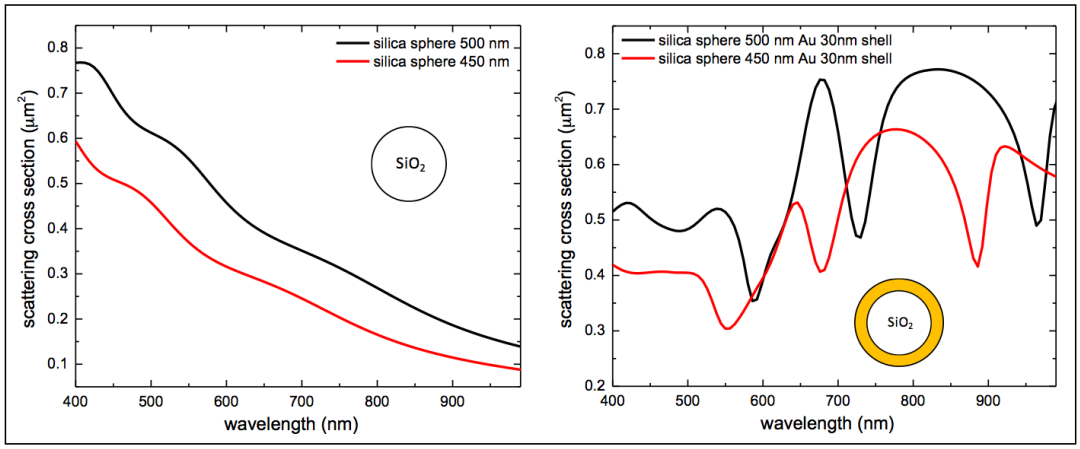

Figure 4.4: Simulation comparison between optical scattering properties of a 500nm silica particle and a metal coated 500nm silica nanoparticle

This forms the basis of our experiment as it can be clearly seen that a thin layer of gold has the capability to change the scattering crossection at different wavelengths.

4.2.2 Microscopic observation methodology

For structural coloring of nanoparticles, the dispersed nanoparticles on a transparent substrate are illuminated using a transmission microscope and scattered light is collected from the top. As seen in Figure 4.6, a sample with and without metal caps are illuminated using the same light source and the structural coloration of particle can be seen. To test our hypothesis that this change is indeed due to the change in particle diameter, we devised a four pronged approach with

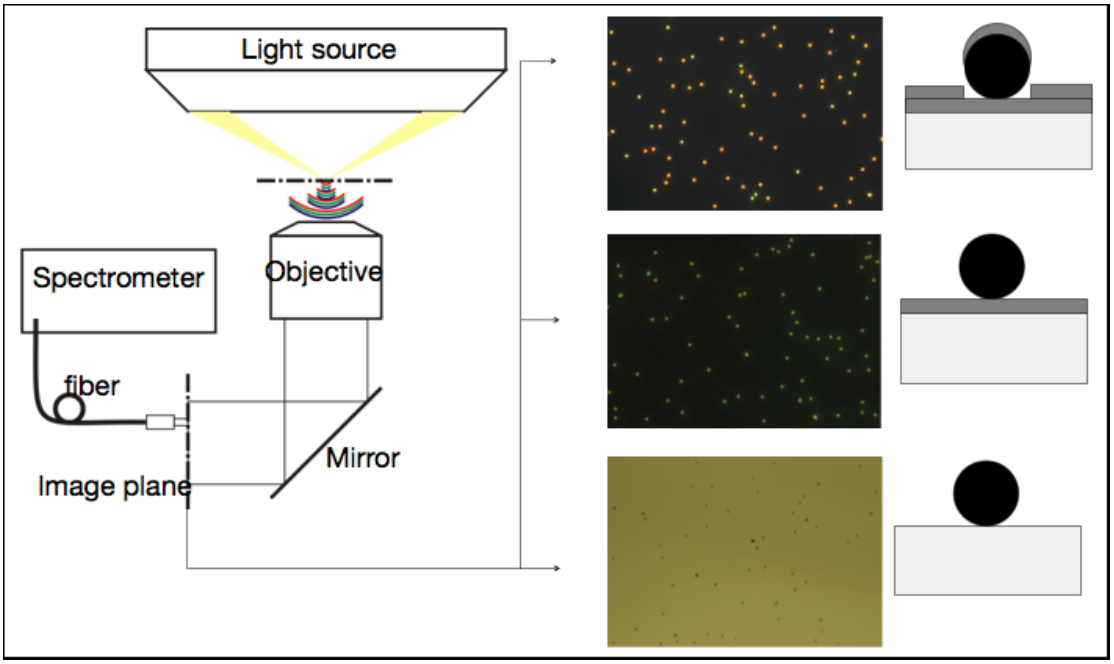

Figure 4.5: Optical observation setup and transmission images of silica particles with and without metallic caps. All images taken under the same illumination.

control samples:

1. Scanning electron microscopy
2. Color detection and characterization
3. Optical spectrum measurement

Under similar conditions and measuring the sizes and optical responses of same particles in all these three conditions can unequivocally validate our methodology to detect relative size variations in nanoparticles by structurally coloring them.

4.3 Material and methods

4.3.1 Fabrication of metallic caps on nanoparticles

Monodisperse silica particles of 525nm diameter were purchased from Sigma Aldrich and aqueous dispersions with a particle density of 10^8 particles/ml were prepared. Fused silica substrates were piranha cleaned and coated with 70nm of Au using physical vapor deposition. Nanoparticle dispersions were spin coated on to these substrates using a three

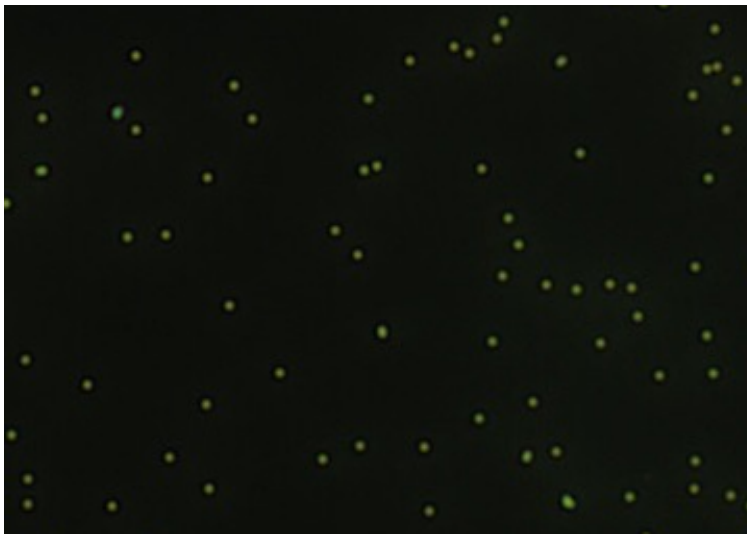

Figure 4.6: Distribution of nanoparticles on substrate after spin coating and first deposition

step ramp: 500rpm for 60s, 2000rpm for 60s and 6000rpm for 10s. This created a good distribution of individual particles on the sample as seen in figure 4.6. This image was taken under a transmission microscope and the green color is due to the

Au film underneath the particles. A secondary Au deposition of 30nm created caps on the particles as seen in figure 4.7. SEM images show the particle with the cap and the aperture underneath.

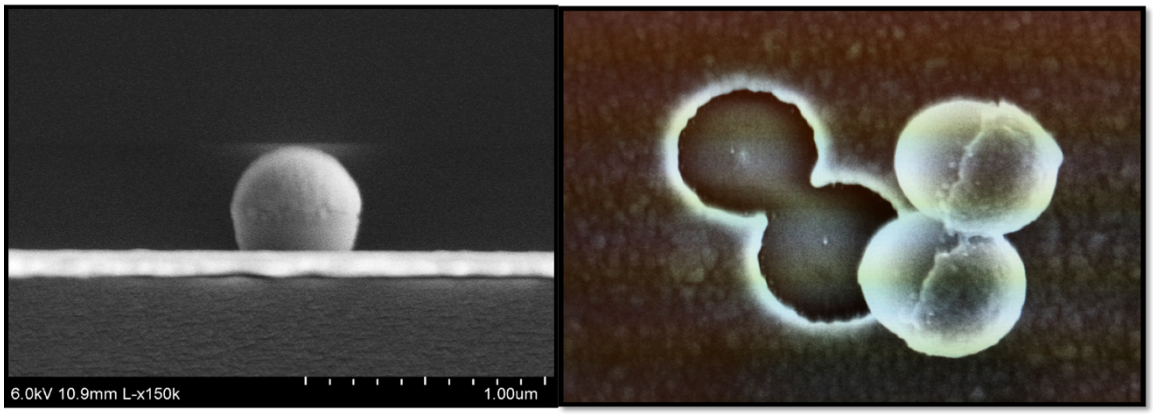

Figure 4.7: SEM images of 500nm silica particles with metal caps. (Left) crossection view. (Right) detached particles showing the aperture underneath

4.3.2 Experimental observation

Samples containing the particles were place on a transmission optical microscope with illumination from a halogen lamp. A dark field condenser was used to collect light, observe color and measure spectrum using an external spectrometer. The coordinates for all tested particles were noted for future reference and to eliminate inconsistencies in the observed color. As seen in figure 4.6, the microscopy setup is described. Color of the particles was acquired using an RGBG CCD connected to a Nikon TE-300 microscope. Images were captured at full resolution of the CCD (3840

x2160 pixels) and further processed using the image analysis toolbox in the Matlab package.

4.4 Relative size characterization of capped nanoparticles

As mentioned in section 4.2, at first we imaged an area of sample with capped nano particles under our optical transmission microscope. Figure 4.8 shows the coloration of monodisperse silica particles. These colors correspond to various resonant

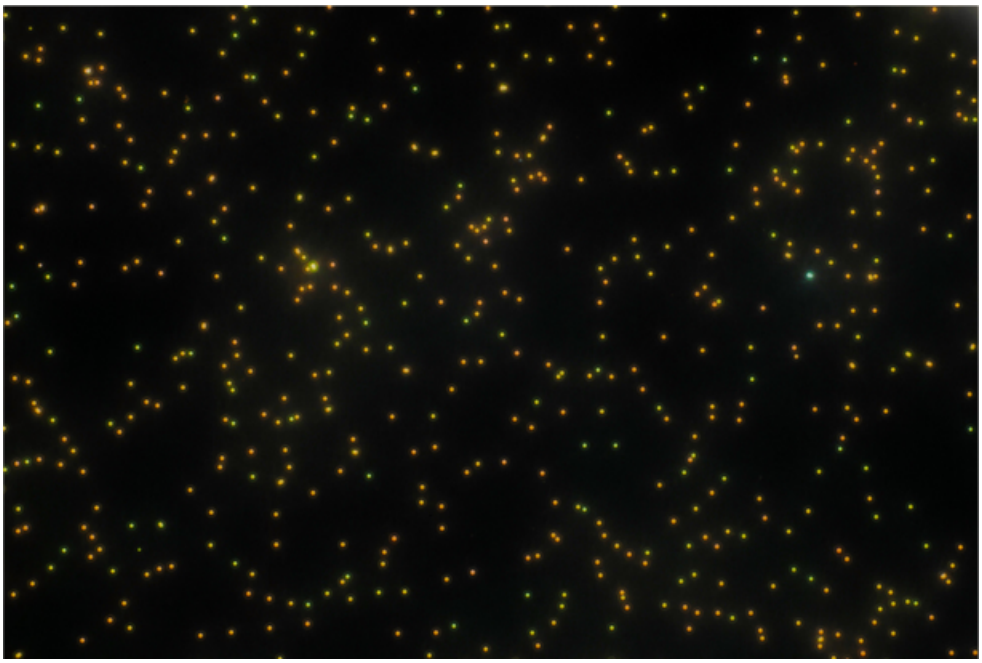

Figure 4.8: Optical transmission micrograph of 500nm silica particles displaying various structural colors

frequencies. A greener particle is smaller in size than a red particle as the resonant peak is red shifted in the latter case. A section of this CCD image was coordinated

and an SEM was used to measure the size of particles individually. Particles were identified in each case and size variation corresponding to color variation was identified. This exemplifies the advantages of our methodology. In case of an SEM we need to individually test the average diameter of each particle where as color variation visualization can easily give us the same information in a fraction of the time.

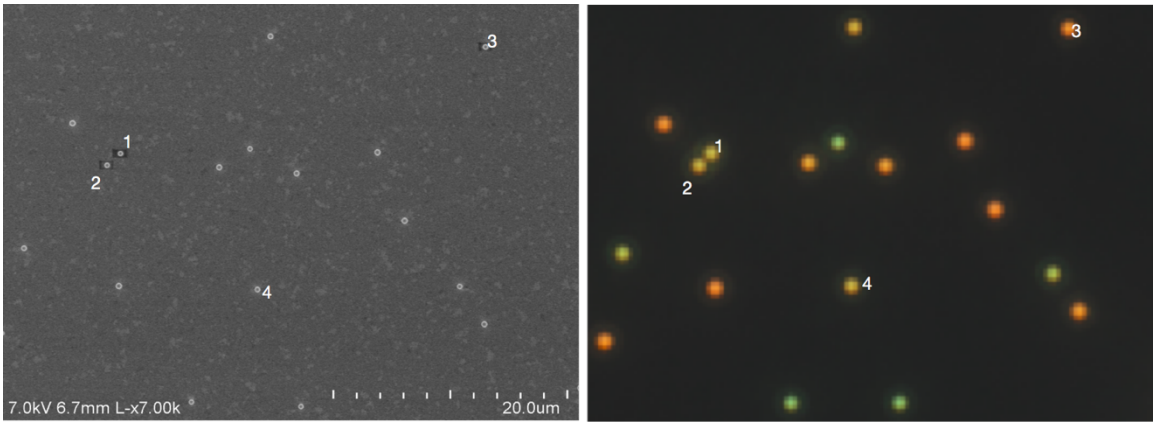

Figure 4.9: Correlation between particle sizes and color using an SEM (left) and an optical microscope (right). SEM measured size (average over horizontal and vertical, WD 4mm) Particle 1: 433 nm; Particle 2: 450.5 nm; Particle 3: 471 nm; Particle 4: 434.5 nm.

As can be seen in Figure 4.9, larger particles are more reddish in color and the smaller diameter particles are more bluish in color. By using image processing algorithms, we were able to capture images from the CCD and analyze the Red (R value), Green (G value) and Blue (B values) of each individual particle in real-time. After analyzing an

ensemble of 30 particles with these two methods, we plotted the red and green values of each particle with the actual diameter measured by the SEM and as can be seen in Figure 4.10, the size distribution is very close to the structural color change. An intuitive assumption was made that a particle with a larger size will have a larger R value.

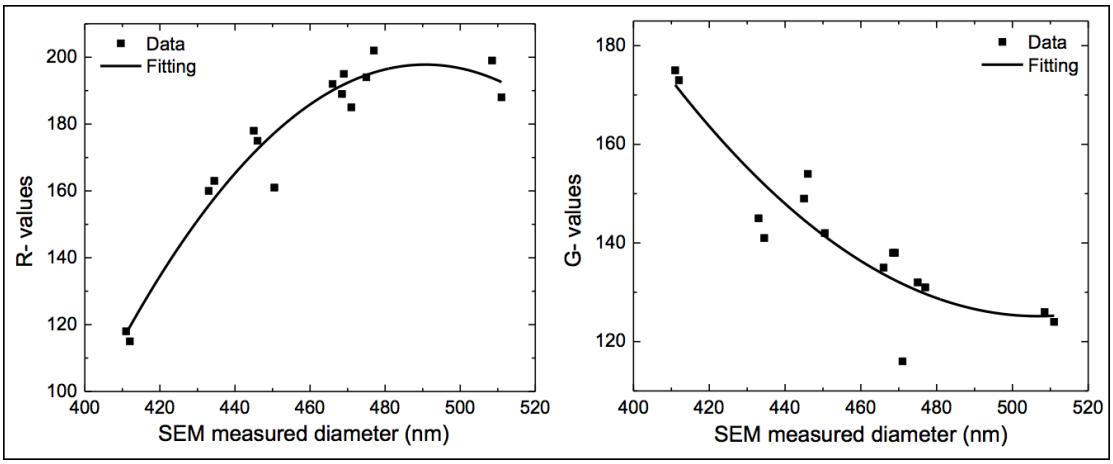

Figure 4.10: Variation of SEM measured diameter with the representative R and G values of the CCD image for the same particles

This provides us with comprehensive evidence that the structural color varies with the size of the particle diameter which in turn depends on the metal cap on the nanoparticles. To test this further, we ran simulations to detect the resonant frequency peaks and then used a high resolution spectrometer to collect the signal from each particle using a 2um diameter optical fiber. Background signal was individually

collected in each measurement. Figure 4.11 depicts how the simulation peaks agree with the optical spectrum of nanoparticles or various sizes

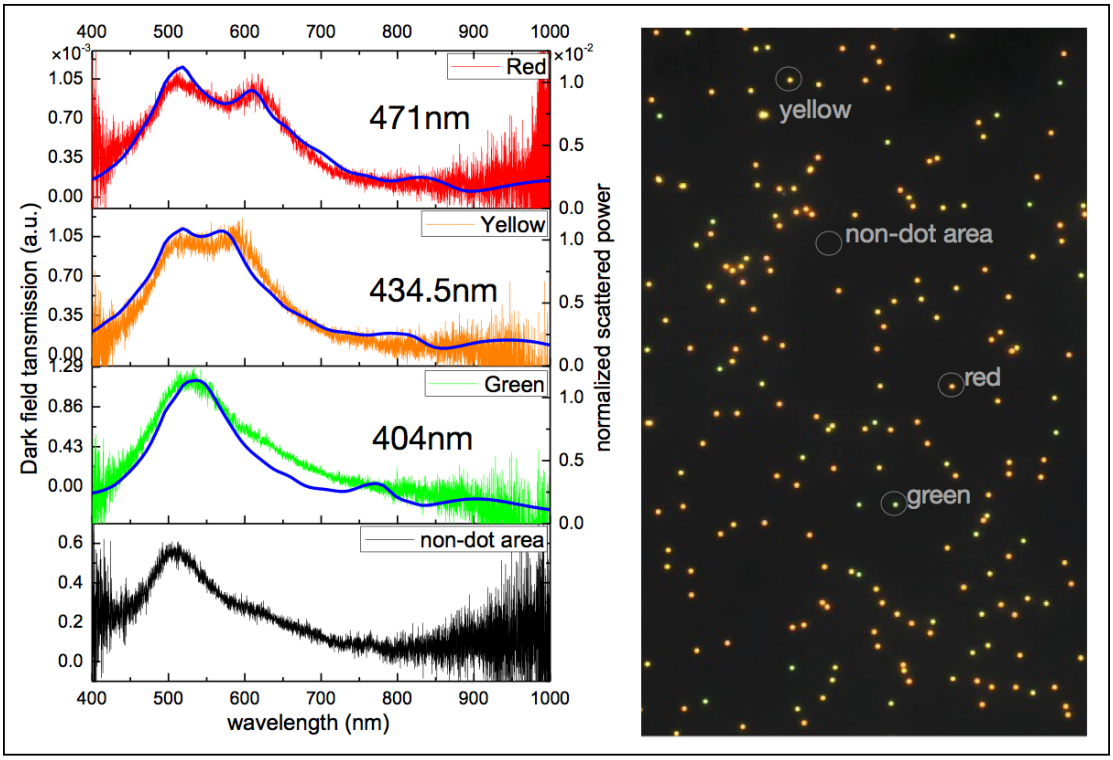

Figure 4.11: Optical response spectrum for 500nm silica particles of red, yellow and green color. Background signal (black) for reference.

The optical response spectrum collected from our spectrometer shows the peak shift as the particle color changes from red to green. The second order peak is of interest to us and it shows the peak shift towards larger wavelength for larger particles and blue shifted for particles with smaller diameter.

4.5 Conclusion and future outlook

Based on the above presented evidence, we have developed a new methodology for detecting relative size variations between nanoparticles differing by as small as 20nm. SEM, optical and spectroscopic measurements agree to confirm that size variations in a nanoparticle ensemble can be detected and visualized using structural colors. It is important that this method is limited to visualizing low-index nanoparticles but not metallic nanoparticles and in our experiments we have used 500nm silica particles and this method could be used to characterize smaller particles too but spectrum measurement becomes extremely hard due to the very low signal to background response. In this way we have created a single-step methodology to visually identify relative size variations in a nanoparticle ensemble that has been pre-characterized using various other methods. We envisage that an automated detection methodology can be developed using the underlying principles mentioned in this capped particle optical sizing methodology presented here.

4.6 References

1. Allen, T. Powder sampling and particle size measurement. (Particle Size Measurements, 1997).
2. Bernhardt, I. C. Particle size analysis: Classification and sedimentation methods. (2012).
3. Searl, A. J. P. M. Syvitski (ed.) 1991. Principles, Methods, and Application of Particle Size Analysis. xiii 368 pp. Cambridge, New York, Port Chester, Melbourne, Sydney: Cambridge University Press. Price £45.00, US $70.00 (hard covers). ISBN 0 521 36472 8. Geological Magazine 130, 400 (1993).
4. Suttiponparnit, K. et al. Role of Surface Area, Primary Particle Size, and Crystal Phase on Titanium Dioxide Nanoparticle Dispersion Properties. Nanoscale Res Lett 39, 20460 (2010).
5. ANDREW M SMITH, S. N. Semiconductor Nanocrystals: Structure, Properties, and Band Gap Engineering. Accounts of chemical research 43, 190–200 (2010).
6. Committee, A. M. Classification of methods for determining particle size. A review. Analyst 88, 156–187 (1963).
7. Gille, W. Particle and Particle Systems Characterization. (CRC Press, 2013). doi:10.1201/b16057
8. Berne, B. J. & Pecora, R. Dynamic Light Scattering. (Courier Corporation, 2013).
9. Wilson, K. & Walker, J. Principles and Techniques of Biochemistry and Molecular Biology. (Cambridge University Press, 2010).
10. Sun, S. F. Physical Chemistry of Macromolecules. (John Wiley & Sons, 2004). doi:10.1002/0471623571
11. Breaking the resolution limit in light microscopy. 5, 289–301 (2006).
12. Rui, L. The mechanisms of electric-dipole spin resonance in quasi-one-dimensional semiconductor quantum dot. Acta Physica Sinica 64, –167303 (2015).

13. Kelly, K. L., Coronado, E., Zhao, L. L. & Schatz, G. C. The Optical Properties of Metal Nanoparticles: The Influence of Size, Shape, and Dielectric Environment. J. Phys. Chem. B 107, 668–677 (2003).
14. Chowdary, M. V. Study of Various Factors Affecting Light Scattering Efficiency of Nanoparticles. 1–19 (2015).
15. Kokhanovsky, A. A. & Weichert, R. Multiple light scattering in laser particle sizing. Applied Optics 40, 1507–1513 (2001).
16. A Primer on Particle Sizing Using Dynamic Light Scattering., NSTI-Nanotech 2006, www.nsti.org, ISBN 0-9767985-6-5 Vol. 1, 2006
17. Scattering Theory of Waves and Particles., By Roger G Newton

CHAPTER V

Nanoparticle manipulation for application in transparent heads-up-display

5.1 Introduction and motivation

Modern displays have become the most prevalent portals for information processing and distribution and most of the information we consume is channeled visually through displays of various forms and sizes[1]. Specifically, commercial automotive research on innovative technologies that integrate with existing advanced driver assistance systems is in its ascendancy. A transparent Heads-up- display (HUD) is one such technology that is in its infancy and requires a specific feature that differentiates it from existing electrophoretic displays. A transparent HUD shows all relevant and contextual information in the line of sight of the driver. There are several factors that interplay in the design of a HUD: field of view, collimation, eye-box, bore sight, luminance/contrast, scaling and compatibility[2]. Unfortunately, amalgams

of these requirements are the challenges faced by existing and prospective technology candidates for transparent displays[3,4]. Our innovation for scattering based transparent displays enables features like wider field of view (FOV), extreme transparency, integration (space constraints) with windshield, low power consumption and an angle insensitive viewing experience. A transparent HUD shows all relevant and contextual information in the line of sight of the driver. It is therefore a key technology in increasing both safety and comfort in the vehicle. Current state-of-the art HUD technologies rely on a reflection based projection system where light travels from the projector and forms a virtual image on the semi-transparent reflector. Due to space

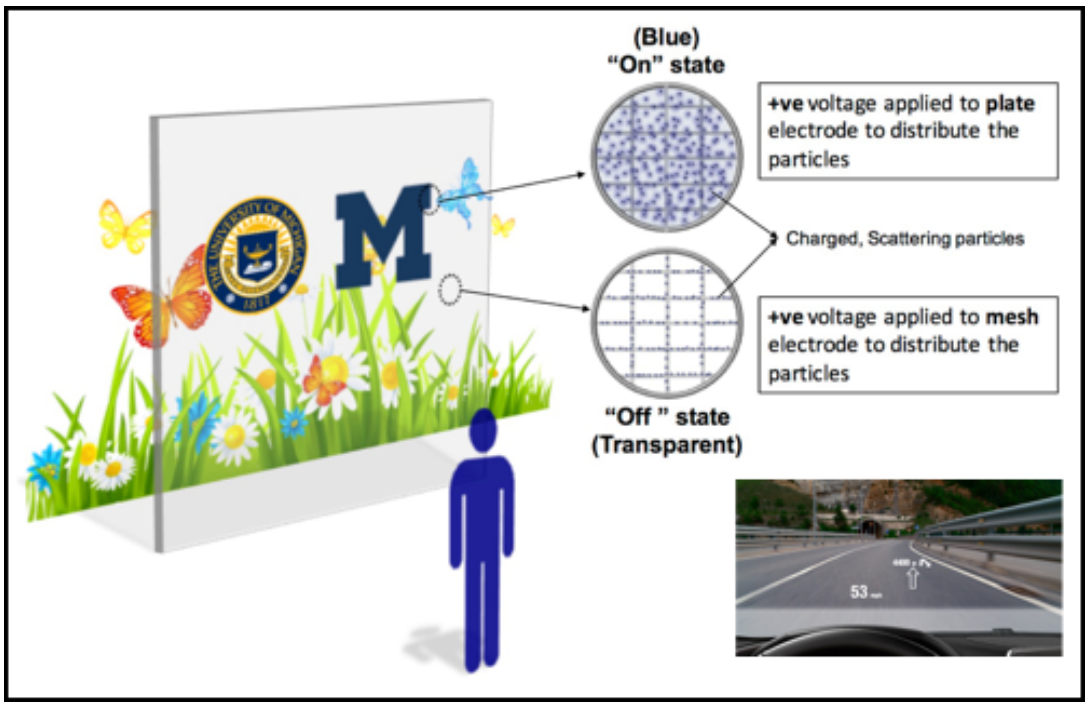

Figure 5.1: Proposed schematic methodology for transparent display based on nanoparticle manipulation in solutions

constraints in a vehicle, these systems are limited in size and the image formed is angle sensitive. The projected images shift with viewing angle, which raises safety concerns when the driver moves his/her head around. The limited space to install the projection system presents another challenge due to the already crowded instrument panels under the dash board. We propose a novel particle-based, field driven and low-power transparent display technology that can be used in ambient lighting conditions. These individual research areas presented in this thesis informed and complimented our transparent display concept as seen in Figure 5.1. Our primary technical challenges to demonstrate this concept was to overcome technical hurdles like stability of particle suspensions, test anti-stiction surfaces and optimize the contrast ratio for outdoor visibility. These challenges are inherent to an electrophoretic display and can be tested independently and cohesively for a better understanding of compromises to make for a display module for a specific market space. It also helps to understand the relationship between optimization parameters based on existing specifications for HUD's.

5.1.1 Electrophoretic display technology

A typical electrophoretic display (EPD) consists of charged particles moving

either towards or away from the viewers eyes in response to an electric field. Electrophoretic displays offer high brightness and contrast across the full range of viewing angles and image bistability.[5] These attributes make electrophoretic displays an attractive candidate for portable devices that require easy readability in a variety of lighting conditions from indoor to bright sunlight without consuming much power. Electrophoretic displays have a long history. Ota et al.[6] first reported in 1973 a display comprised of pigments suspended in a color oil, where DC voltage drove the pigment to the front or the back. In the late 90s, Jacobson and co-workers demonstrated the first example of a microencapsulated EPD[7]. Subsequent work at led to dramatic improvements in performance, and the subsequent availability of active-matrix transistor planes let to mass commercialization. Today, the dominant electrophoretic display cells are manufactured by E Ink Corp., using black and white pigments in a microencapsulated and electrically insulating oil. When a DC voltage is applied to a pixel, the black and the white particles are driven to opposite faces of the pixel, each attracted to a particular charge. The pigments tend to form a solid layer across the face of the microcapsule, with the pigment in the front of the cell hiding the pigment in the back. Continuous gray scale can be achieved by only partially driving the pigments across the cell gap[8]. Some of the key challenges faced by this

technology are: bi-stability of the particles, suspension stability, contrast, color, refresh cycles, particle stiction to surfaces and particle sedimentation. Some common advantages include an appearance that is insensitive to lighting conditions and to viewing angle, lightweight, and low power. The technology continues to advance, becoming higher performance, more reliable, and lower in cost. Dynamic imagery with gray scale remains a major unsolved challenge and if demand for color, transparency, and video becomes high then the current dominance of vertical electrophoretic displays devices could very well be eroded.

5.1.2 Review of current transparent display technologies

While EPDs have historically had the reputation of being slow, a cell with a 50 ms cell response at 15-V operation have been reported[9]. While technically its possible to use combinations of colored pigments to generate color, the best method used so far has been the usage of a black and white particle EPD with a RGBW color filter[10]. The use of a white sub pixel enables a brighter white state but tends to give dark, muddled and poorly saturated. Despite these major advances, a commercial electrophoretic technology with high-resolution color and gray scale comparable to printed media is still lacking. More importantly this technology inherently cannot be

transparent. Furthermore, some of the most promising color e-paper technologies are unable to provide the speed required for advanced touch interfaces or dynamic media. Existing HUD systems rely on a light-reflection based projection systems, where the projected image is displayed on a semi-reflective screen that has low transparency. This display methodology is extremely energy inefficient as the reflectance is ~10% and requires a large amount of space (lenses, lights source, cooling system etc.) under the dash board. The images displayed are angle dependent (5°-10°), have a very small FOV and can be hard to view in bright conditions. From an integration standpoint, there are a lot of components competing for space behind an automotive steering column and because of the high spatial requirements of a projection system. Low-cost, modular HUD's rely on a flip-up display above the dash board but these systems are not popular as it defeats the main purpose of HUD's which is to keep the driver's eye on the road. There are specific transparent display technologies like electroluminescent displays that provide extreme transparency and refresh rate but these displays are segmented and these segments cannot be changed once the display is integrated and hard coded. Electrophoretic display made popular by e-ink rely on a top-bottom approach for displaying information. Although, these displays have high contrast and consume extremely low power, these display cannot be made transparent

without overhauling their key technology principles. Newer micro-display imaging technologies are being introduced, including liquid crystal on silicon (LCoS), digital micro-mirrors (DMD), and organic light-emitting diode (OLED). These current state-of-the-art technologies have a maximum theoretical transparency of 58% and unlike liquid crystal displays, the material costs do not scale with size. Transparent OLED display has only 30% transparency, unsuitable for HUD application. We propose a differentiated and transparent display technology concept that takes advantage of all the benefits of a reflective display and has innovative solutions to make them transparent and dynamic.

5..2 In-plane transparent display methodology

Our transparent display methodology utilizes a horizontal particle suspension movement methodology. Unlike conventional electrophoretic displays, we use a scattering core-shell particles and fluorescent nanoparticles as one embodiment to scatter individual colors based on size without the use of color filters and then use particle suspensions to show or hide this color. As seen in Figure 5.2., our display operates through the lateral movement of particles across a pixel when a potential is applied. This is based on the same principles of our uniaxial confinement

methodology discussed in chapter 2. 1D nanoline electrodes are used to create the mesh electrodes as they reduce non-specific binding onto the mesh and at the same time generating high fields that reduce the response times of driving particle suspensions in solution. Figure 5.3 shows this microscopic interaction.

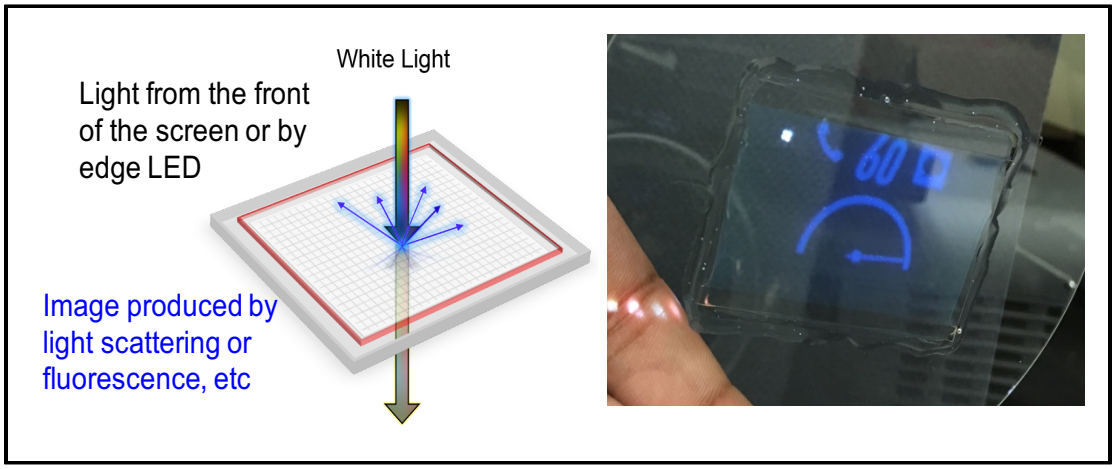

Figure 5.2 Depicts the utilization of Ag core shell particles for scattering based display

The core-shell particles scatter light of a specific wavelength light when distributed across the pixel to produce a colored pixel state. In the light (or cleared) pixel state, the particles are collected onto the voltage-biased electrodes allowing light to be transmitted through the pixel, exposing a reflector underneath or being transparent if a transparent electrode is used on the opposite side. Our display platform is enabled by electric-field driven particle suspensions. This offers fast response times capable

of displaying colorful and video imagery. Our scattering display stacks are extremely thin

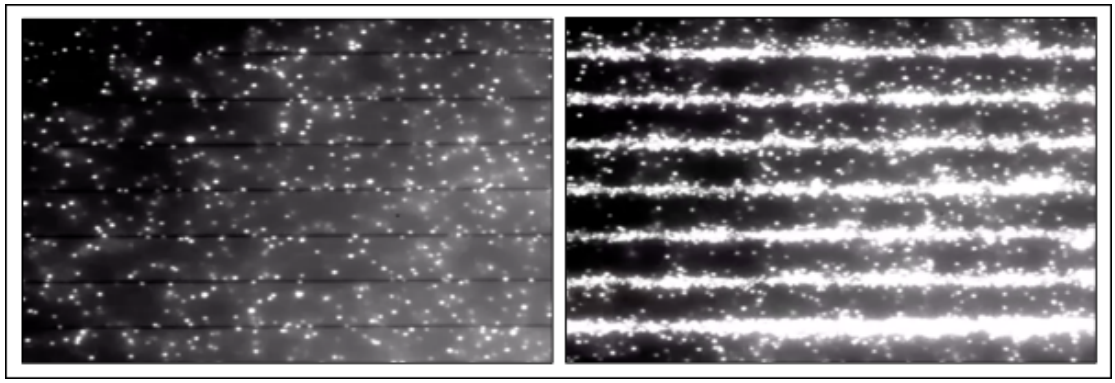

Figure 5.3: Nanoline electrodes with particles dispersed (left). With particles attached to the line electrodes on application of voltage bias.

and efficient and as we use a single particle suspension, we evade many technical issues faced by current electrophoretic technologies. This manipulation of particles using our nanoline electrodes creates the on/off states at the macro scale. 1D nano lines attract nanoparticles of opposite charge and can do that reversibly. By creating line width that was thinner than the particle diameter, non-specific binding was avoided and the particles can be attracted or repelled reversibly. The other advantage of a using a line charge to manipulate particles in solution is that the electric potential well near a line charge is extremely deep and sharp when compared to a planar charge. Therefore, for the same applied voltage, particles can be attracted to the line at a faster rate than on a planar electrode. The plot in chapter 2 Figure. 2.7 shows how

the electrostatic potential energy between the line charge and the particle changes with a distance r between them. For scatter light of a specific wavelength based on the Mie scattering phenomena explained in chapter 4. A proof-of-principle demonstration is shown in figure 5.2, where light scattering particles show an image of a speedometer on transparent fluidic cell.

5.4 Display operation characteristics

Combining the above mentioned features, we created a fluidic device with mesh electrodes and used a transparent ITO as a counter electrode to visualize the ON/OFF states of our transparent display principle. The ON state represents the state in which no electric field is applied and the fluorescent nanoparticles are free to diffuse, displaying a color in the pixel. In the OFF state, nanoparticles are compacted behind the mesh electrodes making the pixel transparent to the viewer (black in case of figure 5.4). As the mesh electrodes occupy only 5% of the viewable area of the pixel, this display geometry is capable of having a transparency as high as 95%. As we use a single particle suspension, we evade many technical issues faced by current electrophoretic methodologies.

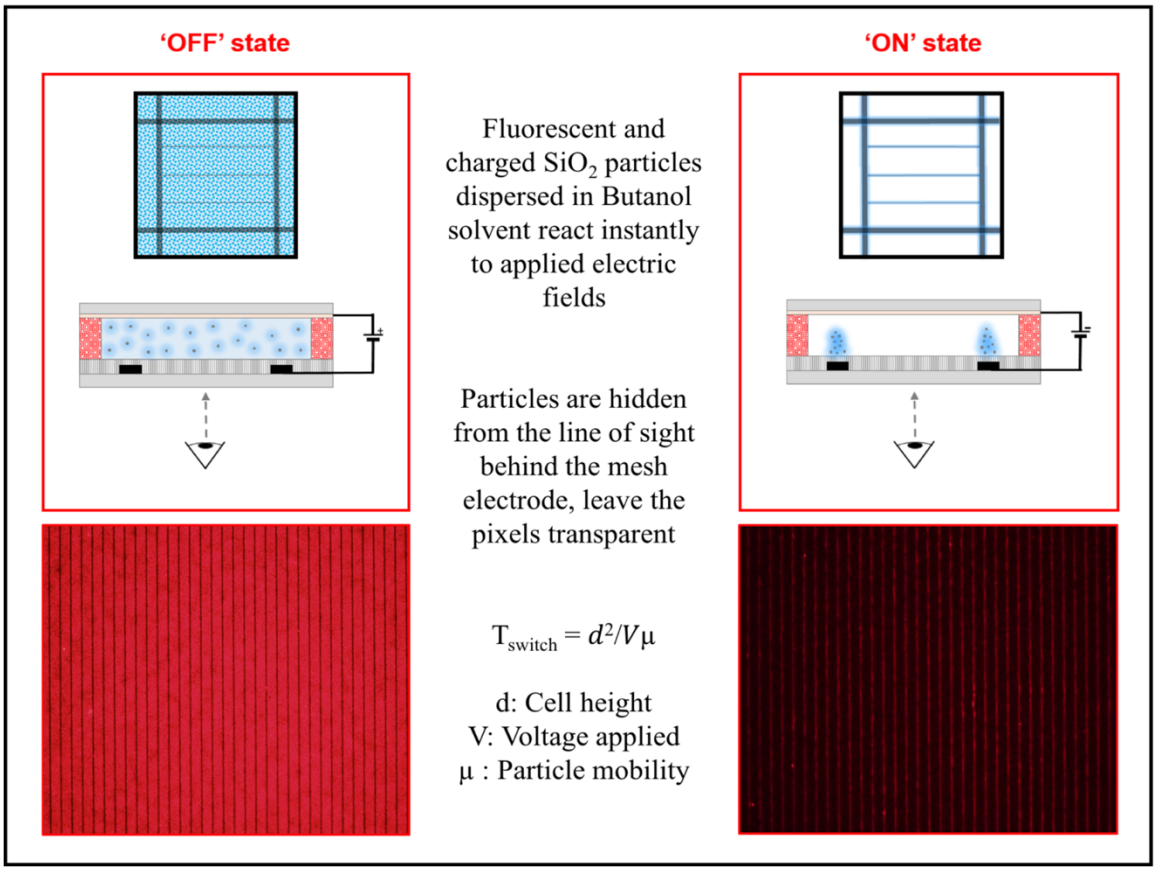

Figure 5.4: Schematic and fluorescence micrographs depicting the ON/OFF states in the fluidic cell as seen by the viewer

Due to its facile fabrication needs, our display geometry can be potentially fabricated by roll-to-roll processing techniques resulting in substantial cost savings. Our technological advancement uses existing manufacturing techniques and uses 80% less material by volume than conventional displays making it extremely economical and sustainable.

5.5 Conclusion and future outlook

In summary we have devised a new method to utilize particle manipulation using electrostatic fields to create a display geometry can be transparent and has high response times and is capable of dynamic imagery. Further study is being conducted to realize a complete actively driven transparent display that can integrate into a HUD unit. Using the concepts presented in chapters 2 and 4, we are able to mitigate some of the challenges faced by existing transparent display technologies. We have also developed a projection based quantum dot film based display that is more accessible from an implementation perspective. Development of large scale prototypes require cohesive process integration steps which will allow us to further test the compatibility between various processes and also address the technical challenges related to scalability and reliability. A working prototype presented here allows us to demonstrate the feasibility of our innovative approach, thus closing the gap between experimentation and implementation.

5.6 References

1. Klein, S. Electrophoretic liquid crystal displays: how far are we? Liquid Crystals Reviews 1, 52–64 (2013).
2. Peng, H. et al. Design and fabrication of a holographic head-up display with asymmetric field of view. Applied Optics 53, H177–H185 (2014).
3. Chien, L.-C. Bistable reflective displays for paper-like displays. 2007 Asia Optical Fiber Communication and Optoelectronics Conference 139–141 (IEEE, 2007). doi:10.1109/AOE.2007.4410730
4. Hsu, C. W. et al. Transparent displays enabled by resonant nanoparticle scattering. Nat Comms 5, 1–6 (2014).
5. Comiskey, B., Albert, J. D., Yoshizawa, H. & Jacobson, J. An electrophoretic ink for all-printed reflective electronic displays. Nature 394, 253–255 (1998).
6. Heikenfeld, J., Drzaic, P., Yeo, J.-S. & Koch, T. Review Paper: A critical review of the present and future prospects for electronic paper. J. Soc. Inf. Display 19, 129–28 (2011).
7. Colorant Transposition Displays. 1–35 (2015).
8. Name, Y. Driving E Ink Displays. 1–35 (2012).
9. Lenssen, K.-M. H. in Handbook of Visual Display Technology 1–15 (Springer Berlin Heidelberg, 2015). doi:10.1007/978-3-642-35947-7_102-2
10. Yin, P. et al. CYM and RGB colored electronic inks based on silica-coated organic pigments for full-color electrophoretic displays. J. Mater. Chem. C 1, 843–849 (2013).
11. Smith, G. N. & Eastoe, J. Controlling colloid charge in nonpolar liquids with surfactants. Phys Chem Chem Phys 15, 424–439 (2013).
12. Guo, Q., Lee, J., Singh, V. & Behrens, S. H. Surfactant mediated charging of polymer particles in a nonpolar liquid. Journal of Colloid And Interface Science 392, 83–89 (2013).

CHAPTER VI

Conclusion

In conclusion, we have demonstrated various methods to confine, manipulate and assemble nanoparticles using electrostatic fields and charge regulation in fluidic systems. In the case of uniaxial confinement of nanoparticles, we see a strong correlation between experimental and theoretically reported order parameters of diffusion. While the experimental evidence on the behavior of charged nanoparticles near a line charge can be substantiated by our experimental demonstration, we envisage that this methodology and the results can fill in the gap that the recent theoretical studies have tried to justify. The central result of this work is to demonstrate mimicking biological interactions in a synthetic system and in the process creating an active, electrostatic trap for confining charged nanoparticles in solution. In the similar way, confining and assembling nanoparticles onto voids opens new possibilities for high throughput filtration systems as our void patterns can be produced in large scale by roll-to–roll manufacturing techniques. Further investigation needs to be done to understand the low fill-ratio of the structures and we envision an active system of controlling particle position by incorporating a layer of metal on the void pattern and biasing against a counter electrode. The relationship between particle size and void structure brings us to the novel methodology that we introduced to visualize the relative size distribution between nanoparticle ensembles and its applications will be useful in research labs that identify particle size as a critical factor in experimentation.

Automating our system using a software database will also make this methodology more accessible. Combining all the above mentioned merits of particle manipulation, we were able to develop a novel transparent display technology that has a commercial application in the automotive industry. Technology commercialization can be challenging and our primary goal with developing a display was to solve some technical hurdles that exist in the industry and with this background understanding of fundamental concepts and applied research we have mitigated some of the challenges associated with existing display technologies. A lot open ended questions still remain in each of these areas and it is my hope that this thesis provides as a building block for further research as various studies in the past have helped in my research as a Ph.D. student at the University of Michigan